Financial risk assessment of the breakwater construction phase

S.W. van Wierst

TU Delft

Van Oord

Marine ingenuity

Cover Image: 'SSDV Frans' at work at project Dubai Maritime City, United Arab Emirates
(retrieved and adapted from Van Oord (2019))

Financial risks assessment of the breakwater construction phase

Feasebility study of a probabilistic process-based simulation model

by

S. W. van Wierst

In partial fulfilment to obtain the degree of Master of Science
at the Delft University of Technology,
to be defended publicly on Tuesday November 12, 2019 at 15:30.

Student number:	4238982	
Thesis committee:	Prof. dr. ir. M. Kok,	TU Delft
	Dr. ir. B. Hofland,	TU Delft
	Ir. T. J. Zitman,	TU Delft
	Ir. G.M. Smith,	Van Oord

An electronic version of this thesis is available at `http://repository.tudelft.nl/`.

TU Delft

Van Oord
Marine ingenuity

Preface

This thesis is the product of several months of research in the final stage of the Master of Science program 'Hydraulic Engineering' at the Delft University of Technology (TU Delft). The subject for this research was formulated in cooperation with Royal Van Oord.

Many people have contributed to the process of forming this report, both direct and indirect. I would like to express my sincere gratitude to the members of my graduation committee, Matthijs Kok, Bas Hofland, Tjerk Zitman and Greg Smith.

First I would like to thank my professor Matthijs Kok, for not only keeping an eye on the bigger picture, but also for always thrusting in me. Secondly, I would like to thank my daily supervisor Bas Hofland, for his endless enthusiasm for anything related to breakwaters and for keeping me sharp on the academic level of my formulations and argumentation. To Tjerk Zitman, promptly available day by day not in the line of duty but with genuine interest. I would you to thank you for your feedback on my work and advice for me as a person.

I would like to thank my supervisor from Van Oord, Greg Smith, for the opportunity to graduate in collaboration with Van Oord. I have experienced this time as extremely instructive and look back on it with great pleasure. I also would like to thank my colleagues at Van Oord, where I could always go, whether it was about sharing their knowledge or just some advice. The fact that during my graduation, the company celebrated its 150th anniversary made it extra special.

Finally, I want to thank the people who supported me during my whole study period. My friends, who were always there for me to spend my free time with. In particular, I want to thank my parents, who supported me mentally and financially during my whole study. Your wise counsel and kind words have, as always, served me more than well.

S.W. (Bas) van Wierst
Delft, November 2019

Abstract

During construction of breakwaters, adverse weather conditions can result in damage, in the form of reshaping and loss of material to the open work fronts of the structure. Removal and (re)placement of dislocated material can be a complicated and time-consuming process, which can induce (severe) delay of the project. Large contractors commonly take out insurance against storm-induced damage during the construction phase. Such construction all risk (CAR) insurance often works with a specified trigger event, e.g. an insurance threshold, which has to be exceeded in order to claim damage. All damage induced by conditions below this threshold contributes to the risk for the contractor.

When a damage event occurs, construction is delayed as repair works are needed. This delay increases the probability of encountering unfavourable conditions in the remaining construction time. Such positive feedback complicates any quantitative risk assessment. The main objective of this thesis is to investigate the feasibility of a computational model with which risks related to the construction phase of rubble mound breakwaters in sea-state conditions can be assessed. While the aim is to keep the mode generic, older breakwater project confronted with storm-induced damage was used as a reference. Before work on the model began, a qualitative analysis is performed to create an overview of the possible damage mechanisms associated with the construction phase. Based on literature research, analysis of work methods, analysis of damage to older breakwater projects and interviews, it was deduced that during construction, the open work fronts of the submerged core section, emerged core section and underlayer section are in particular prone to the following damage mechanisms:

- Reshaping of the submerged core due to head-on and oblique wave attack
- Reshaping of the emerged core due to head-on and oblique wave attack
- Rashaping of the underlayer due to head-on and oblique wave attack.
- Mixing of rock material of different sections.
- Overwash of dislocated material.

To include the earlier mentioned positive feedback in a fully probabilistic risk analysis, a method was created where a fixed time-step stochastic model simulates the construction phase. Simulating the construction process enables it to include the positive feedback between delay due to damage, and the increase in the probability of encountering unfavourable conditions in the remaining construction time. Due to the stochastic behaviour of the parameters used in the building process simulation, the simulation outcome itself is characterised by a stochastic behaviour. To calculate the financial risk, the simulation is run multiple times like a Monte Carlo simulation.

The model checks, per time-step (week), if the randomly sampled least favourable conditions result in damage, as the least favourable condition per time step is decisive for the occurrence of damage. To randomly sample the wave height, probability density functions were determined from the time series, by applying the block maxima method. Subsequently, a parametrised relation between wave height and wave period was determined from the time series, to find a probability density function for the wave period given some wave height. All density functions for the wave characteristic were computed for each meteorological season, to include the effect of seasonality in the model.

To calculate the amount of damage in the model, quantitative damage calculations were performed using methods reported in the relevant literature. While the reshaping of the underlayer can be modelled as a rock armour layer, both the emerged and submerged core section turned out to be more complex to predict. Currently available literature turned out to be limited, as it did not cover all damage mechanisms or the full extent of it. For the emerged core, damage in two particular situations could not be described:

1. The amount of reshaping of the core material in the underlayer section, when the underlayer is breached.
2. Recession of the crest, larger than the initial crest width.

As these two damage mechanisms could not be neglected, two new methods where introduced in the study. They turned out to be to quite promising, as the predictions were very close to the situation of the reference project and other physical tests.

The submerged core can be modelled as a near-bed structure. Depending on the storm conditions, the validity range sometimes became an issue. To solve this issue, an adjustment was introduced, making the make the method applicable for the simulation method.

A Sensitivity analysis was performed to examine which damage mechanisms and breakwater parameters correspond with the largest risk. The relative change of the parameters was compared with the change of the mean financial risk for the contractor and in addition the mean financial risk for the insurance company. The input parameters with the strongest sensitivity on the financial risk were the nominal diameter for core and underlayer material, and the start date of construction works. Although these sensitivity results were obtained using a reference case, there is a strong indication these effects do hold for the general situation.

Concluding from all the result, it is safe to say, that the feasibility of a probabilistic process-based simulation model for quantitative risk assessments is confirmed.

Contents

Nomenclature

Abbreviation

Abbreviation	Full Name
CAR	Construction All Risk
CD	Chart Datum
GEV	Generalized extreme value

Glossary

Chart datum	The water level to which elevations and water depths are reduced.
Damage event	Adverse hydraulic conditions resulting to damage of the breakwater, which requires repair.
Emerged core section	The part of the breakwater during the construction phase, consisting of the open front of the entire core, with an emerged crest.
Insurance threshold	A certain predetermined wave height, which when exceeded during the construction phase, triggers the insurance.
Monte Carlo simulation	The Monte Carlo simulation is a simulation technique in which a physical process is simulated multiple times, each time with different starting conditions. The result of this collection of simulations is a distribution function that displays the entire area of possible outcomes.
Positive feedback	Positive feedback is a form of feedback that positively influences a certain process, with "positive" in the sense of reinforcing, regardless of whether it is favourable or unfavourable.
Reference project	An older breakwater project, where actual damage has taken place due to a severe storm during the construction phase. The reference project is used as a case in this study.
Seasonality	The seasonality or seasonal variation of a time series is the periodic and predictable variation that recur every calendar year.
Submerged core section	The part of the breakwater during the construction phase, consisting of the open front of the submerged core.
Underlayer section	The part of the breakwater during the construction phase, consisting of the open front of the underlayer.
Time series	Series of data indexed with time as parameter.

List of symbols

Symbol	[Units]	Description
α	[deg]	Slope angle
Δ	[-]	Relative buoyant density
$\hat{T}$	[-]	Parameterized period T
μ	[-]	Mean (also called the expected value)
μ	[-]	Location parameter for the GEV distribution
ρ_s	[kg/m^3]	Density rock material
ρ_w	[kg/m^3]	Density water
σ	[-]	Standard deviation
σ	[-]	Scale parameter for the GEV distribution
Θ	[-]	Velocity-based mobility parameter
$\Theta_1\Theta_2\Theta_3$	[-]	Slopes to describe deformed profile in the formulas of Merli
ξ	[-]	Shape parameter for the GEV distribution
ξ_{cr}	[-]	Critical surf similarity parameter
A_e	[m^2]	Area of erosion
$c_{pl,d}$	[-]	Coefficient plunging waves in deep water
$c_{pl,s}$	[-]	Coefficient plunging waves in shallow water
$c_{s,d}$	[-]	Coefficient surging waves in deep water
$c_{s,s}$	[-]	Coefficient surging waves in shallow water
D	[€]	Total amount of damage
D_{15}	[-]	the 15 per cent value of the sieve curve
D_{85}	[-]	the 85 per cent value of the sieve curve
D_{85}/D_{15}	[-]	Grading
D_{ce}	[€]	Damage of the emerged core section
D_{cs}	[€]	Damage of the submerged core section
D_{n50}	[m]	Nominal diameter
D_{UL}	[€]	Damage of the underlayer section
g	[m/s^2]	Gravitational acceleration
h	[m]	Waterdepth
H_{m0}	[m]	Spectral significant wave height
H_0	[-]	Dimensionless wave height parameter
H_0T_0	[-]	Combined dimensionless wave height-wave period parameter
h_c	[m]	Crest height
H_s	[m]	Significant wave height
$H_s(\Omega)$	[m]	Insurance threshold
k	[m^{-1}]	Wave number
L	[m]	Wave length
$L_{of,ce}$	[m]	Length open front, emerged core
$L_{of,cs}$	[m]	Length open front, submerged core
$L_{of,UL}$	[m]	Length open front, underlayer
L_m	[m]	Mean wave length

Symbol	[Units]	Description
M_{50}	[kg]	Median mass stones
N	[-]	Number of waves
$N_{exposure,pld}$	[-]	Number of plunging waves needed breach underlayer, deep water
$N_{exposure,pls}$	[-]	Number of plunging waves needed breach underlayer, shallow water
$N_{exposure,sd}$	[-]	Number of surging waves needed breach underlayer, deep water
$N_{exposure,ss}$	[-]	Number of surging waves needed breach underlayer, shallow water
P	[-]	Notional permeability of the structure
p	[m]	Shifting distance of the local origin to satisfy the massbalance
R_c	[m]	Depth at the crest
S	[-]	True damage number
s^2	[-]	Variance
S_d	[-]	Damage parameter
T_0	[-]	Dimensionless wave period parameter related to D_{n50}
T_m	[s]	Mean wave period
T_p	[s]	Peak period
T_R	[weeks]	Required repair time after damage event
u	[m/s]	Characteristic velocity
u_0	[m/s]	Peak bottom velocity
$V_{e,ce}$	[m^3]	Volume of the eroded core material, emerged core section
$V_{e,ce}$	[m^3]	Volume of the eroded core material, submerged core section
$V_{e,UL}$	[m^3]	Volume of the eroded underlayer material
Z	[-]	Reliability function

1 Introduction

1.1. Research motivation

Throughout the world breakwaters are widely used. These hydraulic structures are primarily designed for the protection of vessels harboured within ports or for port facilities from wave action, but they can also be used to protect beaches from erosion, or to protect valuable natural habitats that are exposed to the destructive forces of the sea. Most of the time these threats come from wave action, however currents and scour can play an important role as well. Without the use of breakwaters it would in many areas not be possible for ships to berth and load their cargo.
In general breakwaters can be devided in four different categories:

- Rubble mound breakwaters, consisting of loose rock material and sometimes concrete blocks.
- Monolithic breakwaters, in which the structure acts as one solid block, like caissons.
- Composite breakwaters, combining a monolithic element with a rubble mound (low-crested) berm.
- Special (unconventional) types, like floating breakwaters and pneumatic breakwaters.

This research focusses on rubble mound breakwaters, as it is the most commonly used type of breakwater. In fig. 1.1(a) a schematic cross-section of a rubble mound breakwater can be seen. It consists of a core ①, often made of quarry run material, underlayers ②, a toe structure ③, an armour layer protecting the whole structure against wave attack ④, and sometimes a crown wall ⑤. As the total structure contains several layers of stone material, where each layer has a different stone diameter, it is not possible to construct the different layers all at once in the same section.

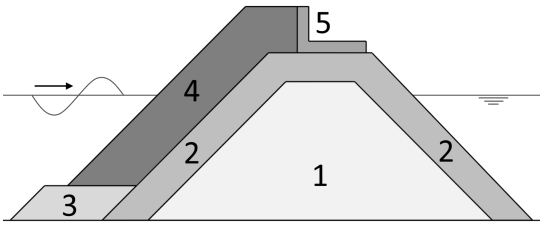

(a) Cross-section

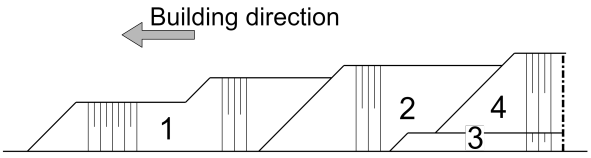

(b) Longitudinal section during construction phase

Figure 1.1: Breakwater components

During construction, the building fronts of the different breakwater components follow each other with a certain distance, this is shown in fig. 1.1(b). The building fronts which later will be covered by another component are called open fronts. The core and underlayers are typically not designed to withstand conditions, with severe or even moderate wave attack, and where the final armour layer of the structure is stable, these underlayers are probably not. In case such a storm occurs during the construction phase, damage in the form of reshaping of the core, reshaping of the underlayers and loss of building material may take place. This undesired reshaping of breakwater components has to be fixed in order to recreate the designed cross-section of the structure. Removal and (re)placement of dislocated material can be a complex and time-consuming process, which most of the time induces delays to the project. Failure of the breakwater in the form of reshaping and loss of building material is a constant risk contractors are faced with, when realizing these hydraulic structures (Smith, 2018).

For the contractor, there is a constant trade-off between building efficiency, and potential damage due to storms. The larger the open work front, the more efficient the building method, as deployment of machinery is less likely to be delayed by slow progress in other sections and therefore shortening the time needed for construction. Comparatively short work fronts, on the other hand, lead to machinery working closer together and a less efficient building method. However the longer the open work fronts, the larger are the vulnerable section areas, increasing damage after a storm drastically. So the trade-off boils down to balancing building efficiency against the risk attended with exposure to storms.

To manage this type of risk, large contractors commonly take out insurance against storm-induced damage during the construction phase. Such insurance often works with a certain trigger event e.g. an insurance threshold. This means that the damage will only be covered by the insurance company if it has been caused by a storm, whose conditions exceeded some predetermined threshold. Nowadays insurance companies tend to ask for more information from the contractor about potential risks before a possible insurance contract is made.

Because of these reasons, Van Oord has shown interest in the development of an instrument which can be used to estimate the risk during the construction phase to a certain extent.

1.2. Problem statement

In this study the risk for the contractor is defined as hydraulic conditions, which do not exceed the insurance threshold, that lead to damage and has to be covered by the contractor itself.

A quantitative assessment of the aforementioned risk is not straightforward. One of the reasons is that the occurrence of damage depends on hydrodynamic conditions, which are not known beforehand. Another reason is that, in general, the longer the construction phase, the more likely it is that unfavourable conditions are encountered. If these lead to damage that needs to be repaired, construction will be delayed, which, in turn, increases the probability of encountering unfavourable conditions in the remaining construction time. This explains the complexity of the problem: it is one big positive feedback loop.

To quantify the concerned risk, where risk is defined as the product of the probability of damage occurring and the cost involved in repairing it, insight is required in:

1. The damage that can be expected as the result of an unfavourable hydrodynamic condition.
2. The probability of occurrence of unfavourable conditions, together with:
3. The mentioned feedback mechanism.

1.3. Objective

As mentioned before, Van Oord would like to have an instrument for the quantitative risk assessment. This not only requires the insight mentioned in section 1.2, but also a method for calculating the risk with a fully probabilistic method, which is able to include the mentioned positive feedback mechanism. The latter is not straight forward, as most risk calculations in hydraulic engineering are done for a fixed lifespan of the structure.

Research aim

The aim is to investigate the feasibility of a model with which risks related to the construction phase of rubble

mound breakwaters in sea-state conditions can be assessed.

To fulfill this objective, we distinguish the following questions to be answered.

Questions

1. What are the damage mechanisms related to the construction phase of a rubble mound breakwater, during storm conditions.
2. How can these damage mechanisms be quantitatively analyzed.
3. How can the positive feedback be included in a fully probabilistic model.
4. Which breakwater parameters and damage mechanisms correspond with the largest risk and uncertainties.

1.4. Methodology and scope

The steps listed below are taken to fulfill the research objective and to answer the research questions.

1. The damage mechanisms of rubble mound breakwaters due to storm conditions are determined qualitatively, based on literature research, analysis of work methods, analysis of damage to older breakwater projects and interviews. Geotechnical failure is not included within the scope of the study.
2. The process behind the mentioned positive feedback mechanism is explained in more detail, and a brief introduction of fully probabilistic methods for risk calculations is given. A model is introduced to include the feedback mechanism within a fully probabilistic risk calculation. It is explained how this fully probabilistic process-based simulation model works, and what is needed to build such a model.
3. The introduction of an older breakwater project. The breakwater dimension and hydrodynamic data are used as a reference to construct the model.
4. Quantitative analysis of how damage can be calculated and how this is put into the model. Here only the currently available literature is used, no physical test will be performed. In situations where available literature is insufficient, an own method is developed and backed as much as possible with available data form the reference project and older physical tests. From this, recommendations will follow where additional research is needed. The focus is on perpendicularly incident waves, as information of oblique wave attack is insufficient.
5. The hydrodynamic data from the case project is analysed to find the correlations between wave variables and to find the (extreme) probability density functions of the significant wave height and mean period, that represents the data best. These correlations and distribution functions will be used by the model to randomly draw hydraulic boundary conditions that correspond with the real situation of the case project location.
6. Determine how damage to the breakwater is repaired and developing a method to determine the required repair time and there associated costs via the calculated damage magnitude.
7. Preforming sensitivity analysis; Different building scenarios are simulated to analyse the sensitivity of different parameters. The different scenarios are also used to find which breakwater parameters and damage mechanisms correspond with the most significant risk and uncertainties.

1.5. outline rapport

This report is structured as follows. The damage mechanisms related to the construction phase are given in chapter 2. Based on literature research, analysis of work methods, analysis of damage to older breakwater projects and interviews, the failure mechanisms are assessed. Chapter 3 explains the positive feedback in more detail and introduces the model for assessing the risk. It explains how this fully probabilistic process-based simulation model works, and what is needed to build such a model. These necessities are treated in the subsequent chapters 4,5,6 and 7. Chapter 4 describes the reference project, which is used as a case in this study. In Chapter 5, the methods for calculating the magnitude of damage, for the damage mechanisms found in chapter 2 are outlined. The focus is kept on perpendicular wave, as information on oblique wave attack is insufficient. Chapter 6 describes how the density functions are obtained from the hydrodynamic

data, and how the non-stationary behaviour due to the seasonality is included. The method to calculate the required repair time and their associated costs are treated in chapter 7. The sensitivity analysis of the input parameters is described in Chapter 8. A discussion on the made assumptions in this study and the obtained results are given in chapter 9. Finally, the conclusion and recommendations are outlined in chapter 10. The appendices give an expended elaboration or more background to different parts of the report.

2

Damage mechanisms

In the problem statement, it became clear, that one of the three uncertainties is how damage develops, given some storm conditions. Here storm is referred as an occurrence of hydrodynamic conditions that cause damage to at least one of the building fronts. To predict the development of the damages, an overview of where damage is possible and which type of damage is important, is a necessity. However, currently available literature on this topic is limited, and other sources By analysing the breakwater construction methods, conducting interviews, analysing damage to older breakwater projects and literature study it was possible to deduce the damage mechanisms related to the breakwater construction phase.

This chapter first will line up the three construction methods in section 2.1, as where damage is possible depends mainly on the open work fronts, and so on the construction method. After that, the damage mechanisms are described in section 2.2. Section 2.3 shows the importance of oblique wave attack. The chapter ends with a conclusion given in section 2.4.

2.1. Building methods

As explained in the research motivation (section 1.1), the components of the breakwater are build in different sections, with a certain distance between the workfronts of these components. Three methods can be distinguished for the construction of these breakwater components: Land-based operations, marine-based operations and a combination of land- and marine-based operations (CIRIA; CUR; CETMEF, 2007). These building methods have different open work fronts. They are introduced briefly hereafter

2.1.1. Land-based operations

In this method, the entire breakwater construction is conducted with land-based machinery. Construction starts from shore and progresses seaward towards the planned locations of the roundhead. The quarry run core is (partially) placed by dump trucks, creating a workfront for other machinery to place the other components. Underlayer, toe-structure, and armour layer are placed by crawler cranes or excavators.

For a land-based operation, the construction equipment must be able to gain access to the crest of the core, and this criterion can dictate its elevation and width. The width should be sufficient for practical execution of the works. Furthermore, lift capacity and the reaching range of the equipment limits the maximum depth of the breakwater and the maximum size of the stones. Despite these limitations, land-based construction is commonly more economic then marine-based operations, especially when transport of material from the quarry to the construction site is done by land (CIRIA; CUR; CETMEF, 2007).

2.1.2. Marine-based operations

Although usually less economic than land-based operations, the advantage of marine-based operations is that they are suitable for larger water depths. On top of that, the marine-based method is indispensable for constructing non-shore connected breakwaters.

Placing of the quarry run core material is done with stone dumping vessels up to a water level that leaves

sufficient depth for the vessels to operate. The core is finished by wheel loaders from flat-top barges or by floating cranes. To trim the slopes and place the underlayer, floating hydraulic excavators and/or floating cranes are used. The toe-structure can be placed using side dumping vessels or floating cranes. Floating cranes are also used for the armour layer.

Compared to land-based operations, marine-based operations are more prone to adverse wave conditions. Being exposed to swell, currents and waves the deployment of floating equipment is more sensitive to delay due to downtime.

In terms of open work fronts the only difference between the land-based and marine-based construction method is that with the marine-based, the core is built in two sections.

2.1.3. Combined operations

For economical reasons most of the breakwaters are build using a combination of the land-based and marine-based operations (CIRIA; CUR; CETMEF, 2007). Just like the marine-based method, the core is build in two sections. First stone dumping vessels place the core up to the minimum draught of the vessel (up to 3 m below the water level, depending on the vessel). Subsequently the core is build up to the required height by land-based operations. Depending on the depth, the underlayer, toe structure and armour layer are placed by land-based or marine-based machinery.

2.2. Damage mechanisms

It is essential to define the term "failure" and "failure mechanism". The term "breakwater failure" is normally used, when the finished structure is damaged such, that it is not able to fulfil its protective function any more. This can be related either to a serviceability limit state or to an ultimate limit state. "Failure" during the construction phase refers in this study to damage that leads to downtime of the project or additional costs. The damage mechanism is the physical process that leads to failure.

To create an overview of all the failure mechanisms related to the construction phase, the combined method is used to distinguish all the different section. By focussing on the combined method, all possible work fronts are included, as land-based, and marine-based slightly differ in open sections. Figure 2.1 shows a schematic overview of the work front sections. During construction, damage can occur at all these sections.

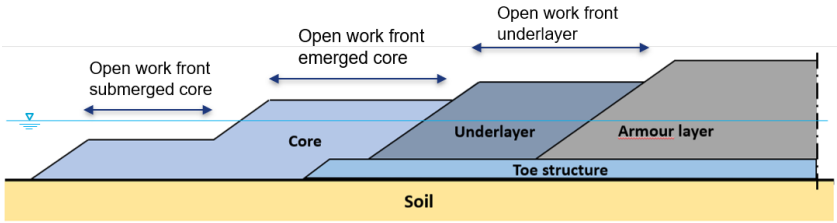

Figure 2.1: Different work fronts of a breakwater, constructed with a combined method.

The armour layer and toe structure of the breakwater are designed to withstand conditions that are exceeded during its projected (design) lifetime with a prescribed maximum probability. These design conditions are way more substantial than the conditions corresponding to the threshold set by the insurance company. This is obvious as insurance loses its purpose if the threshold conditions are larger than for which the structure is designed. Structural failure of the armour layer and toe-structure itself is therefore always covered by insurance, and not of relevance for the research objective. It has to be stated that only a poor design may result in damage of these two breakwater components during construction. However, design faults are not within the scope of this study.

In the following sections the failure mechanisms that may occur during the construction of the emerged core, the subnmerged core and the underlayer are outlined qualitatively (a quantitative description is presented in chapter 5). In all cases, the failure involves displacement of material from the core or the underlayer due to perpendicularly incident waves. The displacement results in a remodelling or reshaping of the cross-section under construction and in some cases in mixing of material from different layers.

2.2.1. Submerged core

Reshaping of the core due to perpendicular wave attack

Depending on the wave height relative to the crest level, waves will break or not. The breaking of waves will result in more damage as energy is leading the profile to spread out (see fig. 2.2). Pysical model tests performed by Van der Plas and van der Meer (2017) show the same reshaping profile as fig. 2.2

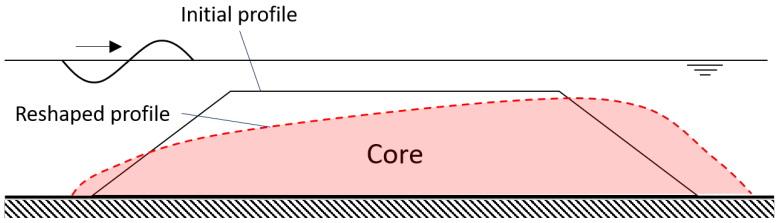

Figure 2.2: Reshaped profile due to severe cross-shore wave attack on the submurged workfront of the core. The red dotted line, shows the reshaped area (pink), the initial (intended) profile is shown with the black line.

Reshaping of the core due to oblique wave attack

From older breakwater projects When attacked by oblique waves the submerged core sections may However information on the stability of near-bed structures for conditions with oblique wave attack is scarce (CIRIA; CUR; CETMEF, 2007). The following studies were done on the stability of submerged / near bed structures: Wallast and van Gent (2002), Van der Plas and van der Meer (2017), All have excluded the effect of oblique wave attack on the structure.

2.2.2. Emerged core

Reshaping of the core due to perpendicular wave attack

The core material is displaced by the waves leading to erosion around the water line, depositing dislocated material at lower levels. When the wave conditions are such that core material is displaced, the shape of the cross-section changes and tends towards an S-type profile typical for an equilibrium with the wave conditions at hand. An example of such a profile is given in fig. 2.3.

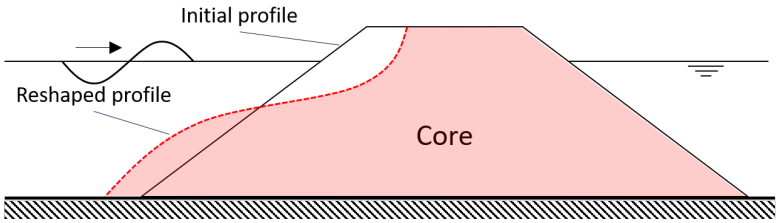

Figure 2.3: Reshaped profile around the still water level, due to perpendicular wave attack on the emerged work front of the core. The red dotted line, shows the reshaped core profile (pink), the intended design profile is shown with the black solid line.

Longshore transport of core material due to oblique waves

When the breakwater is exposed to oblique wave attack, the situation is slightly different than just perpendicular wave attack. Besides the reshaping of the core to an s-curve, there is also transport of core material along the breakwater, adding to the loss of material. The dynamic stability obtained by the reshaped profile may be undermined by this longshore transport, (Mulders, 2010) .

2.2.3. Underlayer

Reshaping

Like the core, the underlayer is also prone to reshaping. However, where it is possible for the slope of the core to reach a stable equilibrium, it is in most cases not possible for the underlayers. The extent in the cross-section of the equilibrium s-shape usually exceeds the thickness of the underlayer. This means that before an equilibrium can be reached, the erosion reaches already the next underlayer in case of more underlayers or the core material in case of a single underlayer. Depending on the severity of the storm at hand, the reshaping

may remain limited to a single layer. In that case, only the slope has to be restored after the storm. This is shown in fig. 2.4.

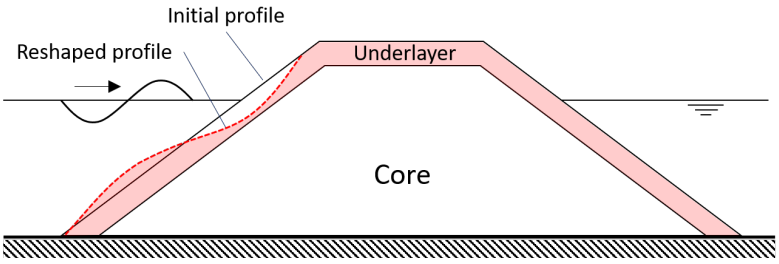

Figure 2.4: Schematic drawing of the reshaped underlayer. The red dotted line, shows the reshaped area (pink), the initial profile is shown with the black line.

Mixing

When the displacement of material develops completely through the underlayer, the core material will be exposed. Erosion will continue with the core and most likely with a higher rate, given the fact that the waves were able to displace the relatively large rocks of the underlayer. Displaced material from the core and underlayer will mix in this process. It is this mixing that creates an extra cost component. As the separation of both materials is economically not possible, the mixed underlayer material is considered lost and new material needs to be purchased.

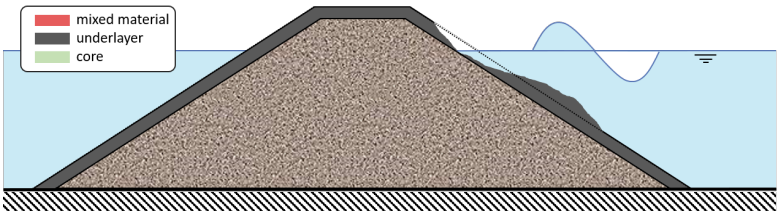

(a) Reshaping of the underlayer

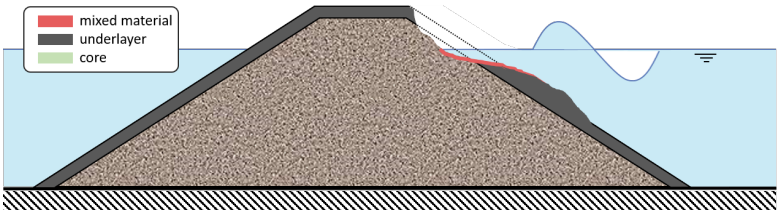

(b) Damage to underlayer and core material, start of mixing

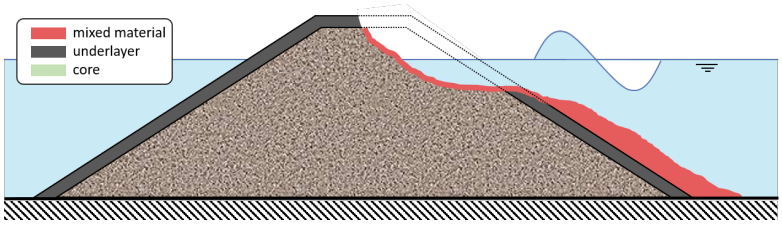

(c) Damage to underlayer and core material, the underlayer of the front slope is fully contaminated with mixed material

Figure 2.5: (a) Wave attack starts to damage the underlayer leading to the reshaping in a S kind of shape. The core material is not yet reached. (b) The underlayer is breached, waves start to damage the core material. The eroded underlayer material starts to mix with the eroded core material. (c) As the wave attack leads to severe damage to the core, the underlayer material erodes with the core. The whole front slope of the breakwater is covered with mixed material.

Overwash

In some situations, the waves can wash the core and underlayer material over the crest. This depends on

the wave characteristics and the water level relative to the recessed crest. Overwash of material leads to deposition on the rear slope. The required repair works depend on how far construction has progressed. In the situation the rear slope only contains core material, the slope needs to be straightened. More costly is the situation where the rear slope already contains the underlayer or even the armour layer, as overwash will result in contamination of these layers, requiring costly repair works to remove the mixed material. In fig. 2.7 a picture of the rear slope is shown where overwash has taken place during the construction phase. In this example, an armour layer had been placed already on the rear slope when overwash occurred. The resulting contamination of this layer is clearly visible in the picture

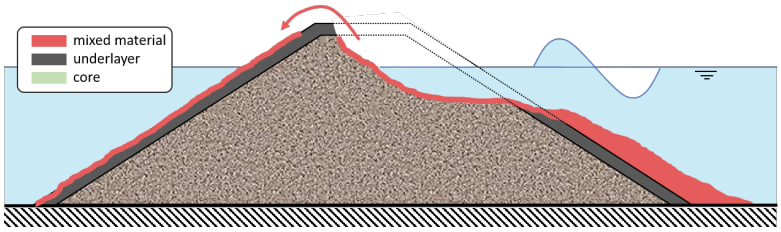

Figure 2.6: Schematic mechanism of overwash.

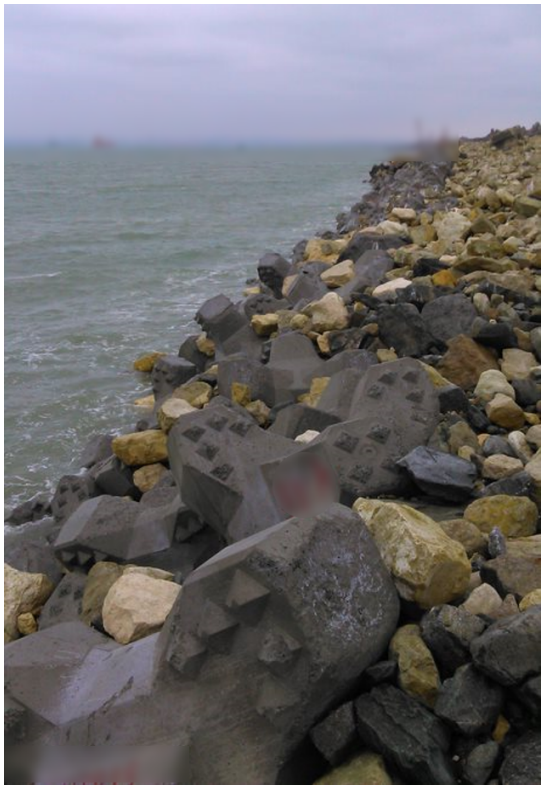

Figure 2.7: Picture of an older breakwater project after a storm had occurred. The rear slope is contaminated with core and underlayer rock material due to overwash (courtesy Van Oord).

2.3. Varying wave direction

The direction of the wave attack is an important parameter for the assessment of damage, during the construction phase. Usually, breakwaters or sections of breakwaters are exposed to waves approaching from different directions. This may have to do with the variability of the wave climate, a curved or bent alignment or a combination of both. This is illustrated in figure 2.8 for a fictitious breakwater. The breakwater in this figure is divided into four parts. During construction all parts will be exposed to the same wave climate, however, the angle of wave attack will be different to each of them, resulting in different possible failure mechanisms and corresponding risks.

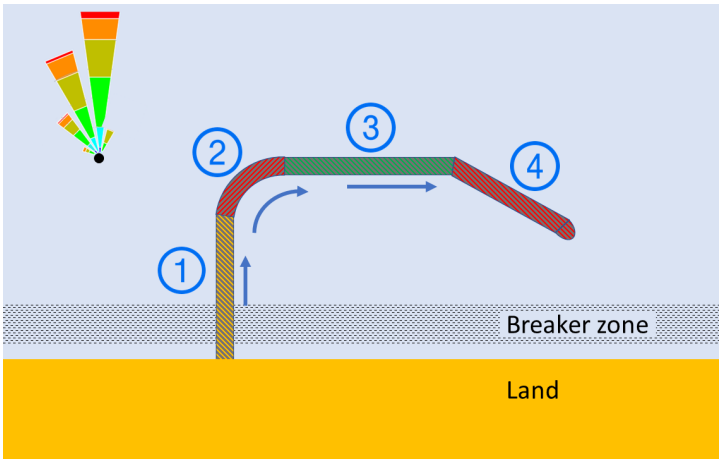

Figure 2.8: Overview of breakwater, where different parts have different angles of wave attack. The arrows indicate the direction of building.

(1) During the construction, this part of the breakwater is exposed most of the time to wave attack head on the open work front (parallel to the length direction of the breakwater section), and very oblique waves attacking both side slopes of the core and underlayer.

(2) The bend section of the breakwater will be exposed to waves perpendicular to the head, but also perpendicular to the side slope.

(3) This part of the breakwater will be most of the time exposed by wave attack perpendicular to the site slope of the trunk, as the waves come from the north/ north-north-west direction. Due to the diffraction and refraction of the waves, this part also faces rear side stability issues.

(4) This part of the breakwater will be exposed to oblique waves when waves come from the northern direction. Waves from the northwest direction will attack form a very oblique direction.

2.4. Conclusion

As described in the methodology, the focus of this study is on wave attack perpendicular on the structure. The main reason for this decision is the leak of knowledge in the current literature on the effect of oblique wave attack on the stability of wide graded structures.

The design conditions for which the armour layer and toe structure are designed for, are far more substantial than the insurance threshold. Insurance loses its purpose if the threshold conditions are larger than for which the structure is designed. Structural failure of the armour layer and toe-structure are therefore always covered by insurance, and therefore not relevant in terms of risk for the contractor.

In the remaining chapters, the study focusses on the following damage mechanisms:

- Reshaping of the submerged core section due to wave attack.
- Reshaping of the emerged core section due to wave attack
- Reshaping of the underlayer section due to wave attack.
- Mixing of rock material of different layers/sections.
- Overwash of dislocated material.

3

Model set-up

In this chapter the simulation model is described. The chapter starts with a brief explanation about the construction all risk insurance in section 3.1. Section 3.2 explains the time dependency of the risk and the process behind the positive feedback between project delay and the probability of a subsequent damage event. With the complexity of the problem known, a method is introduced to estimate the risk by simulating the building process. A short intermezzo on the reliability analysis in hydraulic engineering is given in section 3.3. Section 3.4 gives an introduction to simulations and describes how the model will calculate the risk by simulating the building process of the breakwater. The model output is described in section 3.5 and the conclusion is given in section 3.6 respectively.

3.1. Construction All Risks Insurance

The care of the works is the risk and responsibility of the contractor. As described in the introduction, this risk can be covered by insurance for the works, the Construction All Risks (CAR) insurance.

The insurer will not indemnify the Insured in respect to any loss or damage resulting from adverse sea conditions unless according to the records available the return period of such sea conditions at the project site is higher than the return period of x years (Tanis, 2019). This return period is predetermined and accepted by both parties.

In order to prevent a discussion on what the conditions of a particular return period were, the significant wave height corresponding to this return period is used as a threshold value. Exceeding this threshold, the damage is covered by the insurance company. When speaking of the threshold in the rest of the report, the significant wave height which needs to be exceeded is meant.

The contractor will carry the burden to prove that the threshold is exceeded and exclusion of coverage will not be applied. For this, the significant wave height is measured by observation station(s) within a certain predetermined vicinity of The Works. This leads to two possible events:

- Event leading to damage, where the wave height did not exceed the threshold. Damage is covered by the insured (the contractor).
- Event leading to damage, where the wave height did exceed the threshold. Damage is covered by the insurance company.

So the first point is the real risk for the contractor. From this moment on, when using the term risk, the non-insurable damage events are meant, unless stated otherwise. For more information see appendix B.

3.2. Time dependent risk and positive feedback

Damage due to a storm event, increases the probability of a second storm with a certain return period, occurring during the construction phase. This positive feedback is shown below:

Figure 3.1: Positive feedback of storm damage, on the probability of occurance of second storm.

This increase in probability of a second storm with a certain return period occurring during the construction phase, can be explained relatively simple by the poisson distribution:

$$P = 1 - \exp(-fT) \tag{3.1}$$

In which: P = probability of occurrence of an event one or more times in period T
T = duration of the considered period T
f = average occurance frequency of the event per unit of time

The increase in the project duration results in a higher value of T, and so a higher value of the Probability P. Increasing in project duration can also shift the construction works towards seasons associated with more severe conditions, resulting in a larger average frequency of the event per unit of time (f), and increasing the probability P. For example, the probability of having a storm with a 1/5 year return period, is larger in the winter, than in summer.

To calculate the risk, the interaction between the damage of the first storm and the probability of occurrence of subsequent storms needs to be included. It is this feedback, however, that creates a conflict with the current methods for risk-based design or quantitative risk analyses. In the field of hydraulic engineering, risks or reliability are calculated for a certain fixed lifespan of the structure. Here damage will not influence the probability of subsequent failure events.

Compared to large construction projects within other fields of civil engineering, no situations can be found where damage events increase the probability of occurrence of a second damage event. For example, the construction of tunnels is sensitive to delays due to poor soil conditions and damage to other buildings in the surrounding area. The delay itself, however, does not influence the probability of a second damage event in the tunnel project, as this is depending on the soil properties and not on time-dependent factors. During the construction of a bridge, adverse weather conditions can delay the project. However, where the bridge is different compared to the breakwater, is that all components of the bridge have to be strong enough to stand its given lifetime. There are no more vulnerable sections, like the breakwaters core and underlayer. Thus the construction of bridges can not be compared to the breakwater situation.

Over the years, very limited research has been done on the topic of risk related to the construction phase of breakwaters. Balas and Ergin (2002) developed a Reliability Model for rubble mound breakwaters during the construction phase by taking into account both the structural risks of construction (derived from the wave climate) and other risk parameters arising from problems particular to the construction industry in Turkey. Their work cannot be compared with the current research objective, as it is too limited. The most important limitations are: They only included damage to the armour layer in their reliability analysis, which following from chapter 2 of this research does not represent the actual risk for the construction phase. Furthermore, the positive feedback of project delay on the probability of occurrence of damage events is not included.

In order to predict the risk, the positive feedback has to combined be included into the fully probabilistic approach. Due to the stochastic behaviour of most of the parameters influencing the probability and the magnitude of the damage, a Monte Carlo simulation is needed, as numerical integration becomes to complicated. By simulating the construction process of the breakwater, the effect of delay due to damage can be taken into account. To check if damage occurs, given certain hydraulic conditions, reliability functions will be used. The next section will give a short description on reliability analysis in hydraulic engineering.

3.3. Reliability analysis in hydraulic engineering

The occurrence of damage of a structure is often predicted based on the reliability of the concerned element. This reliability of an element depends on the margin between the resistance and the load or solicitation. The

reliability function (Z) describes this relationship between the strength (R) and the load (S) of an element:

$$Z = R - S \tag{3.2}$$

In reality often both the load and resistance are functions of several stochastic variables:

$$R = R(X_1, X_2, ...X_m) \tag{3.3}$$

$$S = S(X_{m+1}, X_{m+2}, ...X_n) \tag{3.4}$$

Then the reliability function becomes:

$$Z = Z(X_1, X_2, ...X_n) \tag{3.5}$$

The value of the reliability function (Z) describes the state of an element:

$Z > 0$: no failure
$Z = 0$: Limit state
$Z < 0$: Failure

The limit state is a condition beyond which the structure or part of the structure does no longer fulfil one of its performance requirements, hence every Z smaller than zero is seen as failure. Then the probability of failure P_f is defined as:

$$P_f = P[Z < 0] \tag{3.6}$$

Given eq. (3.5) and eq. (3.6), and the fact that R and S are independent the failure probability becomes:

$$P_f = \int \int_{z<0} \cdots \int f_R(x_1, x_2, \ldots, x_m) f_S(x_m + 1, x_m + 2, \ldots, x_n) dx_1 dx_2 \ldots dx_n \tag{3.7}$$

By applying a fully probabilistic method (also known as a Level III method), the probability of failure P_f is calculated, for instance, using numerical integration or Monte Carlo simulations. Solving the problem by numerical integration is limited to simple cases, where the number of variables (n) is small. If the reliability function contains more then two variables, the problem becomes rather complex to solve using analytical formulations or numerical integration, and the Monte Carlo simulation can be used instead.

3.4. Model implementation

As introduced in section 3.2 a simulation of the construction phase is used to predict the financial risk for the contractor. In this section the set-up of the simulation model outlined.

3.4.1. Simulation types

Simulation models can be classified into two simulating methods, namely the continuous simulations and discrete event simulations (Law and Kelton, 2015).

In continuous models, time advances in equal steps and conditions change based directly on changes in time (see fig. 3.2). The system is checked to see if any event has taken place during that interval. All the events which take place during the time interval, are usually considered to have occurred simultaneously at the end of the interval.

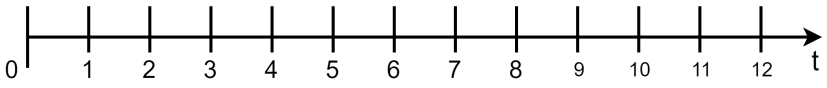

Figure 3.2: Fixed time steps in a continuous model.

Discrete-event simulations, model the operation of a system as a (discrete) sequence of events in time (see fig. 3.3). Each event occurs at a particular instant in time and causes a change of state in the system. Between consecutive events, no change in the system is assumed to occur, hence the simulation time can jump directly to the occurrence time of the next event. An advantage of the discrete event model is that it, in general, requires fewer computations.

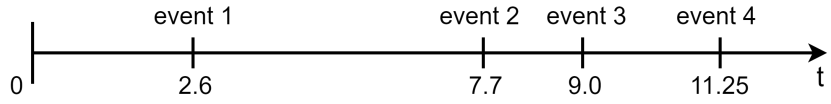

Figure 3.3: Time steps in a discreet event model.

The adverse weather conditions resulting in damage of the breakwater during construction can be seen as discrete events. However, due to the stochastic behaviour of both the strength of the structure and the hydraulic conditions, it is not possible to define a damage event on beforehand, hence a fixed time-step simulation modelling is used in this study. In this study, events which take place during the time interval are considered to have occurred at the beginning of the interval.

The size of the time step is set to one week, as this is considered the most pragmatic: A time step size of one day may be too small, as some damage events (storms) can take up to several days. Times steps of one month are considered too large, as repair works may take less than a month (**?**, **?**), like in the order of weeks. One week is considered to be a representative time step for this purpose.

3.4.2. Interactive fully probabilistic process-based model

With the fixed time step model selected, an introduction on how the model works is given. The simulation of the construction phase goes as follows:

At the begin of the time step, load conditions (H_s & T_m) and stochastic resistance parameters are randomly sampled. It should be noted that the load conditions in the model are a simplification of reality, as the influence of the water level and wave direction are not included. In chapter 4 an explanation is given for excluding the surge. Then these values are put into reliability functions (one function for each section of the breakwater), to check if failure occurs. In this study, failure is defined as the start of damage. If no damage takes place, all the breakwater sections will increase in length with one week of construction progress (see fig. 3.4), and the model goes to the next time step. In the case damage has occurred to one or more sections of the breakwater, the model calculates the magnitude of this damage. Here the amount of damage not only depends on the load and resistance parameters but also on the length of the open front of the breakwater sections. The required number of weeks needed to repair the damage is determined using the magnitude of the damage and certain repair capacities. Until the repair is finished, the progression of the breakwater is on hold. This process is continued until the breakwater is finished. In the model, the breakwater is finished if the required amount of weeks of progress equals the nominal project duration. The nominal project duration is the number of weeks required to build the breakwater in case no delay occurs.

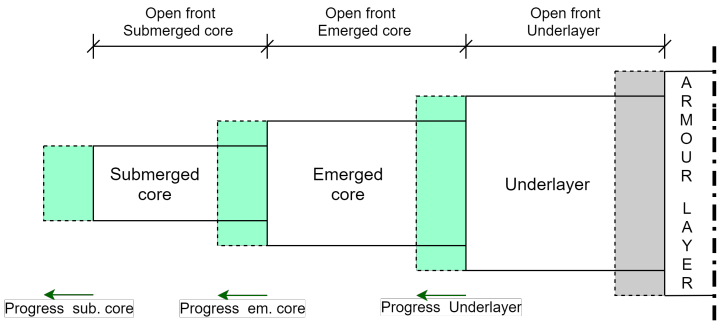

Figure 3.4: A schematic top view of the breakwater with the open fronts of the submerged core, emerged core and underlayer. The green area shows the progress of the construction of one week, when no damage has taken place. If damage has taken place, the progress equals zero, until the required time to repair the damage has been passed. The progress of the armour layer (gray area) follows the other sections with the same progress speed.

The flowchart in fig. 3.5, shows a more detailed overview of the process behind the simulation of the breakwater construction.

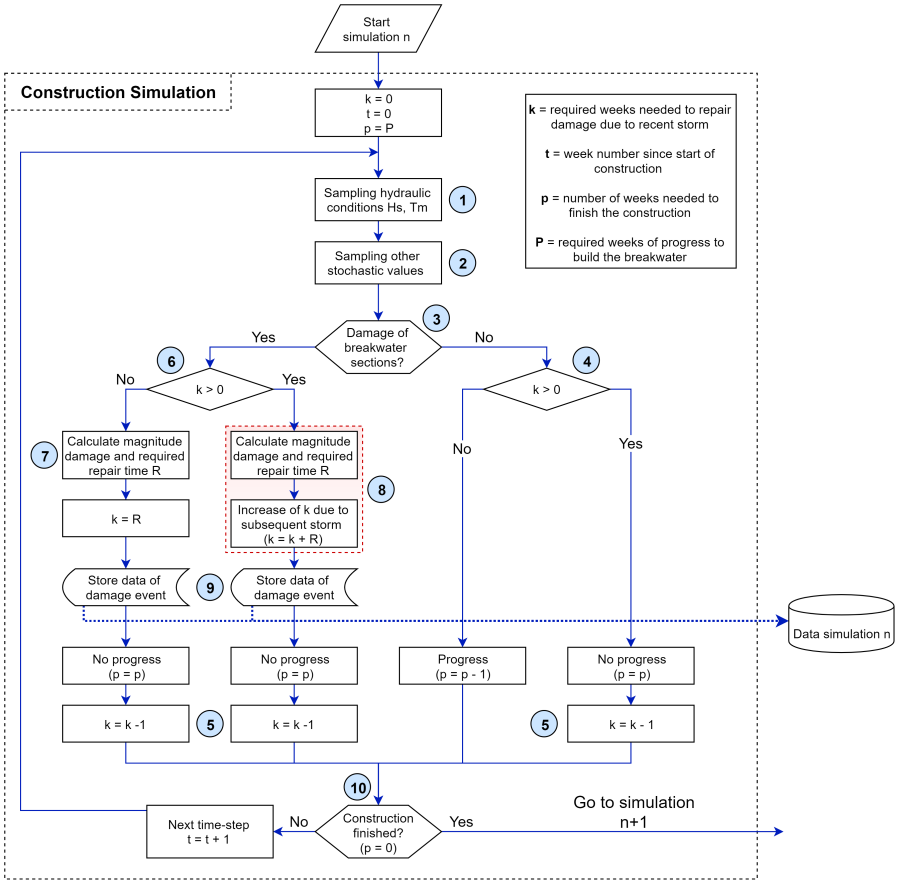

Figure 3.5: Flow chart of the simulation process.

For some steps in the flowchart, indicated with a number behind the process, an extra explanation is provided. These explanations are shown below:

1. Random sampling of the hydraulic conditions H_s and T_m. The methodology on the sampling of hydraulic boundary conditions is found in chapter 6.
2. Random sampling of all the other parameters with a stochastic behaviour, see appendix A for all the stochastic parameters. Chapter 8 provides more insight on which distribution functions are used to represent the stochastic behaviour of the non-hydraulic parameters.
3. The sampled variables are used in reliability functions to check if damage occurs. Chapter 5 goes more into depth onto these reliability functions.
4. Check if repair work due to a recent storm is ongoing. If not, the number of weeks needed to finish the structure will decrease with one, as one week of progress can take place. In repair works due to a recent storm is still on going, no progress takes place and the number of weeks needed to finish the structure will remain the same.
5. The number of weeks required to repair the damage due to a recent storm decreases with 1 week.
6. Check if the occurred damage happens during the time, repair works for a previous damage event are still ongoing.
7. Calculate the magnitude of the damage, chapter 5 goes more into depth on the damage calculations. The required number of weeks for repair work can be calculated using the amount of damage and the repair capacity of available machinery at the project location. From the required repair time, the

financial damage is computed. More insight on the repair time and financial damage can be found in chapter 7.

8. Repair works for a previous damage event are still ongoing. The new required number of weeks needed to repair damage due to recent storms becomes; the required repair time for the current damage event, and the remaining weeks needed for the previous storm.

9. The data concerning the damage event is stored. This data will later be used to calculate the risk. In section 3.5, the specific data which is stored after every damage event can be found.

10. Check if the structure is finished. If not, the model goes to the next time step and will start sampling again of the hydraulic conditions. When the construction phase is finished, the model goes to the next simulation.

Stochastic parameters

3.4.3. Monte Carlo simulation over process-based model

Due to the stochastic behaviour of the parameters used to simulate the construction of the breakwater, the simulation outcome itself is characterised by a stochastic behaviour. To quantify the risk associated with the construction phase, the process-based simulation is put into a Monte Carlo simulation. The Monte Carlo will simulate the construction phase N times, so that the prediction of the risk can be given.

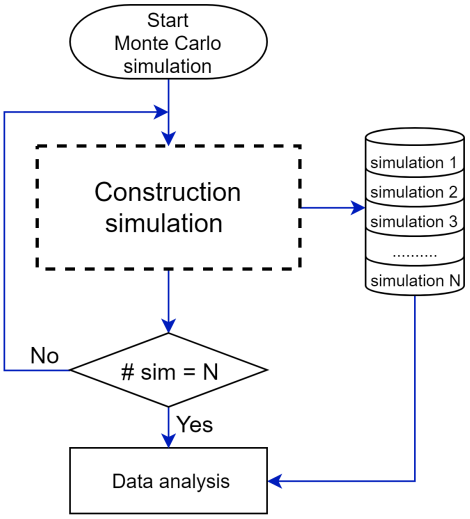

Figure 3.6: Flowchart of the Monte Carlo simulation. The MC repeats the construction simulation N times.

3.5. Model output

3.5.1. Output process-based simulation

During each construction simulation, the model will store certain data when damage occurs. Table 3.1 shows which data is stored after each damage event. When the building simulation is finished, the data is stored until the Monte Carlo simulation is finished. The

Table 3.1: Model output for construction simulation.

Damage event	Hs	Tm	Total damage	D, underlayer	D, core em.	D, core sub.	Repair time
1	$H_{s,1}$	$T_{m,1}$	D_1	$D_{UL,1}$	$D_{ce,1}$	$D_{cs,1}$	$T_{R,1}$
2	$H_{s,2}$	$T_{m,2}$	D_2	$D_{UL,2}$	$D_{ce,2}$	$D_{cs,2}$	$T_{R,2}$
3	$H_{s,3}$	$T_{m,3}$	D_3	$D_{UL,3}$	$D_{ce,3}$	$D_{cs,3}$	$T_{R,3}$
...	...	...	...	...	...	...	...
...	...	...	...	...	...	...	...
M	$H_{s,m}$	$T_{m,m}$	D_m	$D_{UL,m}$	$D_{ce,m}$	$D_{cs,m}$	$T_{R,m}$

3.5.2. Output Monte Carlo simulation

During the Monte Carlo simulation the data from each building simulation is stored. When the MC is completed, the model calculates per building simulation the total non-insurable damage and the insurable damage. The insurable damage and non-insurable damage can be computed by the following formulas:

Total insurable damage:

$$D_{insured} = \sum_{j=1}^{m} (D_j | H_{s,j} \geq H_s(\Omega)) \tag{3.8}$$

Total non-insurable damage:

$$D_{not\ insured} = \sum_{j=1}^{m} (D_j | H_{s,j} < H_s(\Omega)) \tag{3.9}$$

Where:

$D_{insured}$	=	Insured damage	[€]
$D_{not\ insured}$	=	Non-insurable damage	[€]
H_s	=	Significant wave height	[m]
$H_s(\Omega)$	=	Insurance threshold	[m]

Table 3.2: Output of the Monte Carlo simulation part of the Model

Simulation	Project duration	Total Damage	Total Damage, not insurable	Total Damage, insurable	Chance
1	T_1	D_1	$D_{1,ni}$	$D_{1,i}$	1/n
2	T_2	D_2	$D_{2,ni}$	$D_{2,i}$	1/n
3	T_3	D_3	$D_{3,ni}$	$D_{3,i}$	1/n
...	...	...	...	...	...
...	...	...	...	...	...
...	...	...	...	...	...
N	T_n	D_n	$D_{n,ni}$	$D_{n,i}$	1/n

The mean risk for the contractor is the not insurable damage caused by the (Hs < Hs(Ω)). Using the created dataset, the mean risk for the contraction can now be computed by:

$$R = \sum_{i=1}^{n} \frac{D_{i,ni}}{n} \tag{3.10}$$

3.6. Conclusion

From the model description, it becomes clear what knowledge is needed to build the model. First, a reference case is needed to set up the model, Chapter 4 introduces and describes this reference case. Secondly, some methods are needed to check if damage occurs given certain wave conditions and how the magnitude of this damage is calculated. Chapter 5 provides more insight into these damage calculations. To random sample hydraulic conditions, certain distribution functions are needed. Chapter 6 lines out, how the wave data of the reference project is used to obtain theoretical distribution functions which represent the data best. In chapter 7, the method to calculate the required repair time is lined out.

4

Reference project

In order to set up the model, a reference project is introduced. The reference project is an older project, where actual damage has taken place due to a severe storm during the construction phase. In this chapter, the reference project is introduced. Due to confidential reasons, project information and data will be presented and used anonymously.

4.1. Brief description

The reference project concerns a 1050 m long breakwater. The location has a water depth of 25 m, and the wave system is characterized by a wind sea. Chart datum is at -0.2m MSL.

During construction, damage affected by storm events with a significant wave height of 3.5 m or higher was covered by the CAR insurance.

4.2. Dimensions

4.2.1. Cross-section Reference project

In fig. 4.1 the cross-sectional design of the reference project breakwater is shown. The core consists of 1-500 kg quarry run material and the seaside underlayer consists of 1-3 ton rocks at the trunk and 2-4 ton at the roundhead.

4.2.2. Model cross-section

As described in chapter 2, the focus is on the submerged-core section, emerged-core section and the underlayer section. So a cross-sectional design containing only these three sections is needed in the model. For modelling reasons some simplifications of the cross-sections have to be made:

1. The cross-sectional shape of the core will be a isosceles trapezoid, hence the front and rear slope will be straight line.
2. The crest of the core and underlayer will be horizontal straight lines. No level differences within the crest will be include.
3. The underlayer covers the core uninterrupted, no crown element is included.

Figure 4.2 shows the cross-section, which will be used in the model. The submerged core ① is build up to -6.0m. The emerged core ② is built by land-based methods up to +5.0m, and the underlayer ③ up to +6.8m. The core consists of 1-500 kg quarry run material and the seaside underlayer consists of 1-3 ton rocks at the trunk.

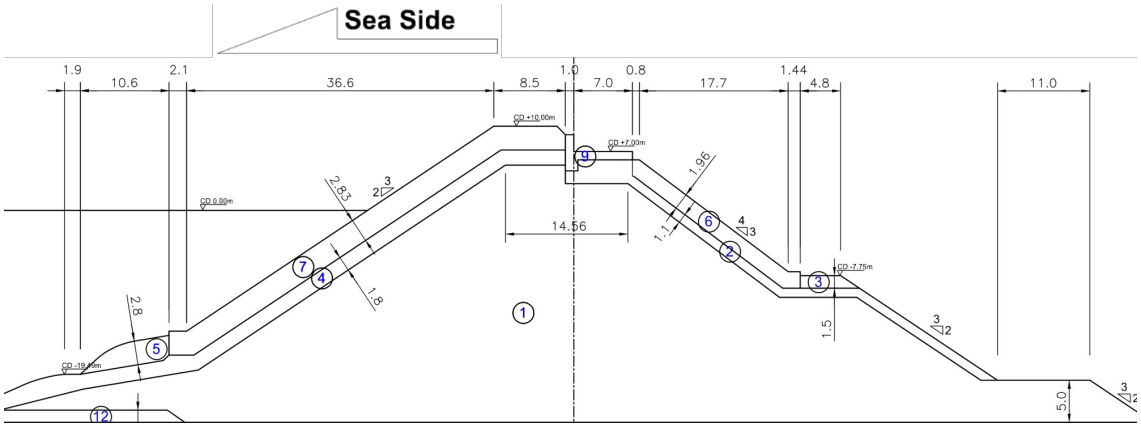

Figure 4.1: Cross-sectional design of the reference project (courtesy Van Oord).

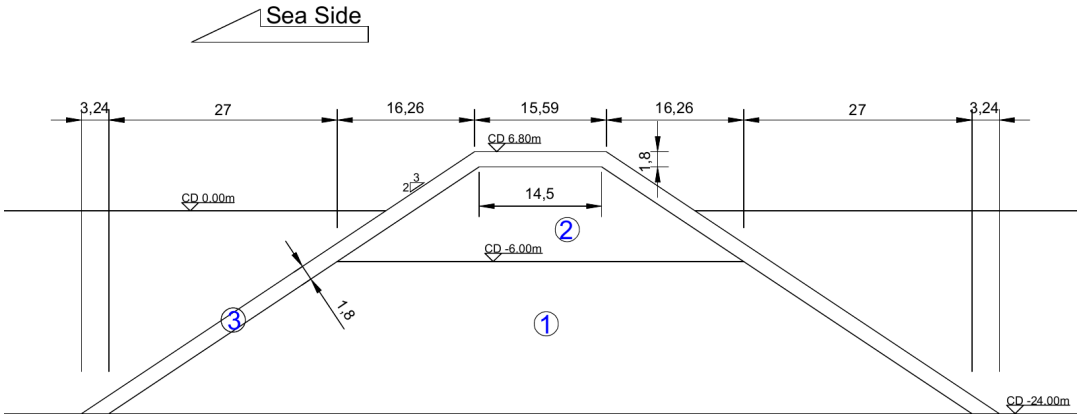

Figure 4.2: Cross-sectional design of the reference project.

4.3. Wave climate

4.3.1. Hydrodynamic data

For obtaining the hydraulic boundary conditions for the model, a dataset of offshore data near the project location is used. This dataset consisted of a 6-hourly time series of 16 years (1997-2013) of offshore wind and wave data.

The data is from the ECMWF hindcast model and has been calibrated to satellite observations and in-situ measurements where available. The location of the offshore data has a water depth of 68m, and since the toe of the breakwater is at a depth of -25, both locations are considered to be in deep water. Therefore the spectral significant wave height H_{m0} is considered the same as the significant wave height H_s.

The 16-year time series does not include measured water levels. According to the design wave conditions report(internal documents Van Oord, 2013), the maximum storm surge is +0.96 m, compared to the water depth of 25 m this is very small. Furthermore, the difference between storm surge of a 1/1 year storm event and a 1/50 year storm event is only 0.2 m. As the water level is missing in the 16-year time series and the surge is relatively small compared to the water depth in the situation of the reference case, the storm surge is not included for the reference case.

4.3.2. Storm event

The storm that hit the breakwater during the construction phase, had the following characteristics:

- A duration of 3 days

- A significant wave height H_s of 4.97 m
- A mean wave period T_m of 7.85 s
- A peak period T_p of 10.53 s

The average angle of wave attack during the storm was 7°, which comes close to direct wave attack. Therefore, the reference project is considered a valid case to consider for direct wave attack.

5

Quantitative damage calculations

5.1. Introduction

In chapter 2 the most important damage mechanisms where distinguished. This chapter focusses on how the amount of damage can be quantified for these mechanisms, when hydraulic conditions are known. Section 5.2 covers the underlayer, section 5.3 does this for the emerged core section and section 5.4 covers the submerged core section.

5.2. Underlayer section

During the construction phase, a part of the underlayer will be unprotected a certain time interval, until the armour layer is placed over it. As the underlayer consists of a specific rock class, it can be seen as a rock armour layer itself. For the stability calculations of loose rock slopes, Hudson and later van der Meer have done valuable research.

5.2.1. Literature

Hudson introduced the stability number $H_s/(\Delta D_{n50})$ and provided four formulas to describe the stability of a rock armour layer. Around 1985, an extensive research program started in the Netherlands in order to overcome the limitations of the Hudson formula and arrive more generally applicable formulas for rock armour stability. This work has led to the van der Meer formulas (1988). Advantages of these formulas are that they include: the effect of the storm duration, the wave period, the permeability of the structure and a clearly defined damage level, of which the latter is essential for this research. A distinction is made between deep water and shallow water conditions. Depending on the surf stability number or breaker parameter, there is a formula for plunging waves and one for surging waves. The following formulas are used to predict the stability:

Deep water
Deep water is defined as $h > 3H_{s-toe}$.

For plunging waves ($\xi_m < \xi_{cr}$):

$$\frac{H_s}{\Delta D_{n50}} = c_{pl,d} P^{0.18} \left(\frac{S_d}{\sqrt{N}} \right)^{0.2} \xi_m^{-0.5} \tag{5.1}$$

For surging waves ($\xi_m \geq \xi_{cr}$):

$$\frac{H_s}{\Delta D_{n50}} = c_{s,d} P^{-0.13} \left(\frac{S_d}{\sqrt{N}} \right)^{0.2} \sqrt{\cot \alpha} \xi_m^P \tag{5.2}$$

Where:

$$\xi_{cr} = \left[\frac{c_{pl,d}}{c_{s,d}} P^{0.31} \sqrt{\tan \alpha} \right]^{\frac{1}{P+0.5}} \tag{5.3}$$

$$\xi_m = \tan \alpha \sqrt{2\pi H_s / (g T_{m0,2}^2)} \tag{5.4}$$

$$\Delta = \frac{\rho_s}{\rho_w} - 1 \tag{5.5}$$

Where:

H_s	=	significant wave height	[m]
T_{M0}	=	mean wave period	[s]
u_w	=	wind velocithy	[m/s]
h	=	water depth	[m]
F	=	fetch lenght	[m]

Reliability of the formulas
The van der Meer formulas are derived empirical with curve fit parameters $c_{pl,d}$ and $c_{s,d}$l. The reliability of the formulas depends on the differences due to random behaviour of rock slopes, the accuracy of measuring damage and curve fitting of the test results. The reliability of eq. (5.1) and eq. (5.2) can be expressed by giving the coefficients $c_{pl,d}$ and $c_{s,d}$ a normal distribution with a certain mean value and standard deviation. The coefficient $c_{pl,d}$ can be described by a mean value of 6.2 and a standard deviation of 0.4 (variation coefficient 6.5%) and the coefficient $c_{s,d}$ by a mean value of 1.0 and a standard deviation of 0.08 (8%).

Shallow water

To make the formulas of van der Meer more applicable in shallow waters, Gent et al. (2004) modified it by using $T_{m-1.0}$ instead of T_m, including $H_{2\%}$ in the formulas and recalibrated the $c_{pl,s}$ and $c_{s,s}$ parameters by model tests. These formulas are displaced below for plunging and surging waves:

For plunging waves ($\xi_m < \xi_{cr}$):

$$\frac{H_s}{\Delta D_{n50}} = c_{pl,s} P^{0.18} \left(\frac{S_d}{\sqrt{N}}\right)^{0.2} \left(\frac{H_s}{H_{2\%}}\right) \xi_{m-1.0}^{-0.5} \tag{5.6}$$

For surging waves ($\xi_m \geq \xi_{cr}$):

$$\frac{H_s}{\Delta D_{n50}} = c_{s,s} P^{-0.13} \left(\frac{S_d}{\sqrt{N}}\right)^{0.2} \left(\frac{H_s}{H_{2\%}}\right) \sqrt{\cot\alpha}\, \xi_{m-1.0}^{P} \tag{5.7}$$

Reliability of the formulas
In the modified van der meer formula the parameter values are also modified. $c_{pl,s}$ = 8.4, with a standard deviation of 0.7, and $c_{s,s}$ = 1.3 with a standard deviation $\sigma_c s, s$ of 0.15. The mean values of the $c_{pl,s}$ and $c_{s,s}$ does not differ that much with the ones van der Meer provided for shallow waves, the standard deviations however increased. It suggests that the inclusion of the new shallow water tests have increased the scatter in the results, and therefore increased the uncertainty of the formula.

5.2.2. Reliability functions

In order to check if failure takes place, the fully probabilistic method (level III), requires reliability function. The shown design formulas in section 5.2.1 need to be transformed into reliability functions. In the van der Meer formulas, the nominal stone diameter (D_{n50}) is seen as the resistance (R), as it indicates the strength of the structure. The load is defined as the significant wave height (H_s) divided by the remaining parameters in the formula. This results in the following reliability formulas:

Deep water
For plunging waves ($\xi_m < \xi_{cr}$):

$$Z = D_{n50} - \frac{H_s}{\Delta c_{pl,d} P^{0.18} \left(\frac{S_d}{\sqrt{N}}\right)^{0.2} \xi_m^{-0.5}} \tag{5.8}$$

For surging waves ($\xi_m \geq \xi_{cr}$):

$$Z = D_{n50} - \frac{H_s}{\Delta c_{s,d} P^{-0.13} \left(\frac{S_d}{\sqrt{N}}\right)^{0.2} \sqrt{\cot\alpha}\, \xi_m^{P}} \tag{5.9}$$

Shallow water
For plunging waves ($\xi_m < \xi_{cr}$):

$$Z = D_{n50} - \frac{H_s}{\Delta c_{pl,s} P^{0.18} \left(\frac{S_d}{\sqrt{N}}\right)^{0.2} \left(\frac{H_s}{H_{2\%}}\right) \xi_{m-1.0}^{-0.5}} \tag{5.10}$$

For surging waves ($\xi_m \geq \xi_{cr}$):

$$Z = D_{n50} - \frac{H_s}{\Delta c_{s,s} P^{-0.13} \left(\frac{S_d}{\sqrt{N}}\right)^{0.2} \left(\frac{H_s}{H_{2\%}}\right) \sqrt{\cot\alpha} \xi_{m-1.0}^{P}} \tag{5.11}$$

In the table 5.1 below, an overview of the values for the parameters of the stability formulas (deep- and shallow water) is shown.

Table 5.1: Specific parameters van der Meer formula for armour stability

Variable	Distribution	Mean (μ)	Standard deviation (σ)	5% limit value
Plunging coefficient, deep water ($c_{pl,d}$)	Normal	6.2	0.4	5.5
Surging coefficient, deep water ($c_{s,d}$)	Normal	1.0	0.08	0.87
Plunging coefficient, shallow water ($c_{pl,s}$)	Normal	8.4	0.7	7.25
Surging coefficient, shallow water ($c_{s,s}$)	Normal	1.3	0.15	1.05
Notional permeability (P)	Normal	0.3 - 0.5	0.03 - 0.05	-

5.2.3. Damage calculation

According to Van der Meer (1988), the damage to the armour layer can be expressed as the eroded area around the still water level. If this erosion area is related to the size of the rock, a dimensionless parameter is created which is independent of the size of the structure (slope and height). This damage level is defined as:

$$S = \frac{A_e}{D_{n50}^2} \tag{5.12}$$

Where:

A_e = area of erosion [m^2]

In fig. 5.1 an example of a structure with damage is shown. Van der Meer gave two physical descriptions of the damage level S. It is the number of squares with size D_{n50} that fit into the eroded area. The other description is the number of cubic stones with a size of D_{n50} that eroded out of a D_{n50}-wide strip of the slope. However, depending on the porosity, the grading of the rock, and the shape of the rocks, the actual number of eroded stones within the strip can differ from S. On average the actual number of eroded stones within this D_{n50}-wide strip is between 0.7 and 1.0 times the damage S. More inside in this fluctuation is not available, to prevent the underestimation of the damage, factor 1 is selected.

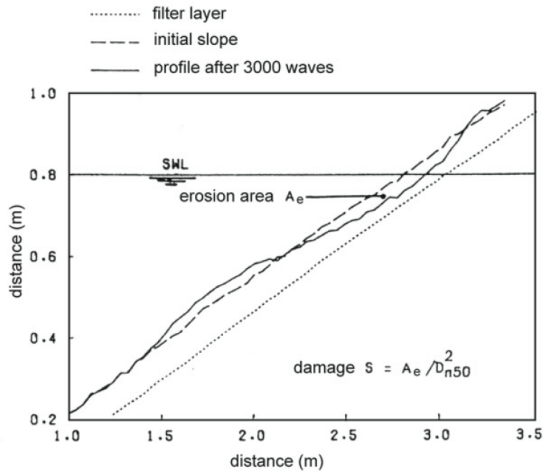

Figure 5.1: Damage level S[-] based on erosion area A_e[m$_2$] (van der Meer, 1998).

For calculating the damage, the actual damage value is needed. Because the reliability function only checks if damage has occurred, given $S_d = 2$, the actual value for S_d can by higher while still resulting in a Z value equal to zero. This actual damage number will be defined as S, to prevent possible confusion with S_d.

The actual damage number can be obtained by rewriting eq. (5.8) as a formula for S and set Z equal to zero, resulting in the following formula:

$$S = \left(\frac{H_s}{\Delta c_{pl,d} P^{0.18} D_{n50} \xi_m^{-0.5}} \right)^5 \sqrt{N} \tag{5.13}$$

Once S is known, the eroded area can be obtained by rewriting eq. (5.12) to :

$$A_e = S D_{n50}^2 \tag{5.14}$$

By multiplying the eroded area with the lenght of the open section of the underlayer, the total volume of eroded underlayer material can be calculated:

$$V_{e,ul} = A_e L_{of,ul} \tag{5.15}$$

Where:

$V_{e,ul}$	=	Volume of the eroded material	[m^3]
L_{of}	=	Length of the open front	[m]

Described in chapter 2, mixing of the core material and underlayer material will occur if the erosion of the underlayer reaches the core. Van der Meer (1988) stated that for damage levels $S > 8$, the material covered by the underlayer started to be exposed. So when calculating the damage to the underlayer, the last step is to check if $S > 8$. If this is the case, the damage now includes the cost for repair works and the additional material costs as the eroded underlayer needs to be replaced.

From the moment the underlayer is breached, erosion will continue with the underlying core material. The quantitative damage calculations for the core material is treated in section 5.3.

5.2.4. Process overview

The flowchart in fig. 5.2 shows the process which needs to be followed in a fully probabilistic approach, in order to check if damage occurs and if so, the magnitude of the damage. In chapter 7, the exact method to calculate the repair costs and material costs will be introduced.

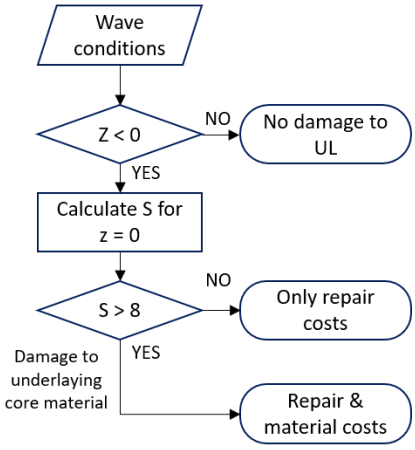

Figure 5.2: Flowchart of the process for quantitative damage calculations for the underlayer.

5.3. Emerged Core section

5.3.1. Literature

Most of the rubble mound breakwaters have a core which typically consists of quarry run with a wide gradation up to 500kg or 1000kg (CIRIA; CUR; CETMEF, 2007).

crest recession

For berm breakwaters, the berm is allowed to reshape. To prevent exposure of the underlying layers, the berm should be wider than the expected crest recession. Over the years, multiple studies have been performed on the crest recession of berm breakwaters. Both Tørum et al. (1990) and Kao and Hall (1990) have studied the relation between the crest recession and the grading of the armour stone. Appendix C goes more into detail into these studies and why at the moment the formulas for crest recession are not sufficient for calculating the amount of damage. Nevertheless, both studies show the importance of the grading on the crest recession. Hence, it should not be neglected.

Reshaping profile

The deformation parameters derived by Van der Meer (1988) can be used to describe the deformation of rubble mound slopes. In his study, however, van der Meer only included gradings within the range between 1.25 and 2.25. Described in Tørum et al. (1990) and Kao and Hall (1990), the grading of the material is of significant importance for the amount of reshaping. Quarry run rock material usually has a grading around 7 or 8 and is considered (very) wide graded material.

Merli (2009) expanded the data set by conducting tests in a wave flume to investigate the effect of grading. For this purpose only tests with head-on waves were executed within a range for grading of 2.7-17.7. Merli adjusted the relations, found by Van der Meer, using curve-fitting to take into account the influence of stone grading. Six parameters were directly defined related to the parameters of van der Meer. The local origin is defined as the intersection between the reshaped profile and the mean water level:

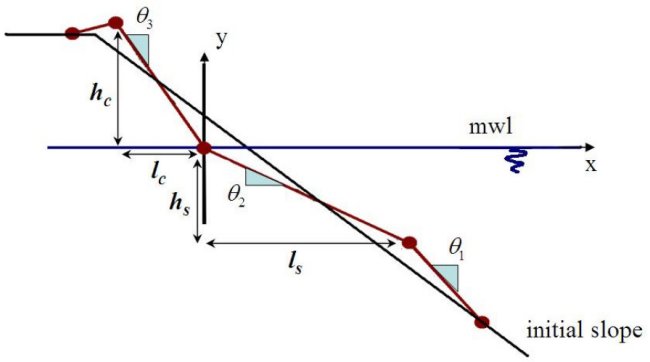

Figure 5.3: Reshaping profile with deformation parameters according to Merli (2009).

- l_s [m]: horizontal offset between the step (below mean water level) and the local origin
- h_s [m]: Vertical offset between the step (below mean water level) and local origin.
- l_c [m]: Horizontal offset between crest (above mean water level) and local origin.
- h_c [m]: Vertical offset between crest (above mean water level) and local origin.
- Θ_1 [-]: Slope connecting the step to the original profile.
- Θ_3 [-]: Slope of the line between the local origin and the observed crest. As it is the ratio between l_c and h_c, its used to calculate the value for h_c. It is fairly independent of the height of the breakwater above mean water level and allows for an estimation of the recession of the crest regardless of the initial height.

These three parameters are computed with the following parameters:

$$H_0 T_0 = 1.66(l_s/D_{n50}N^{0.07})^{1.3}\left(\frac{D_{n85}}{D_{n15}}\right)^{-0.15} + 29.1\cot(\alpha_2) - 9.38 \tag{5.16}$$

$$(H_0 T_0 - 183)\cot\alpha_1 = 139(l_c/D_{n50}N^{0.12})\left(\frac{D_{n85}}{D_{n15}}\right)^{-0.29} - 667 \tag{5.17}$$

$$\Theta_3^{-1} = 0.00023\left(\frac{D_{n85}}{D_{n15}}\right)^{1.58}(H_0 T_0)^{0.84} + 1.5 \tag{5.18}$$

The remaining parameters are computed according to Van der Meer (1988).

The deformation profile is obtained by calculating the seven deformation parameters. Next, the local origin is shifted over the still water level, until the mass balance between the initial profile and reshaped profile is reached.

5.3.2. Reliability Function

During the construction of the core, small reshaping is happening frequent, as the core material consists of (very) small rocks. Minor reshaping of the core around the water level is no problem. Before placing the underlayer material, an excavator will straighten the slope of the core back to the intended shape.

Where static stability has a clear distinction between stability and instability, or failure and no failure, dynamic stability has no such thing. In order to define a reliability formula, a distinction has to be made until what level of reshaping it is not considered as damage. Damage implies serious repair works. This can be translated to the question: from what amount of horizontal shifting of the local origin, it is considered as damage.

Neither Merli or Van der Meer provided a method in their report, to solve the mass balance by shifting the local origin horizontally. What is known is that both used an iterative process to obtain the horizontal shift of

the local origin. An iterative process is very unpopular within a process-based model, as for each time-step, an iteration has to be done, increasing the number of computations drastically.

In order to solve the mass balance, a trigonometric method is composed.

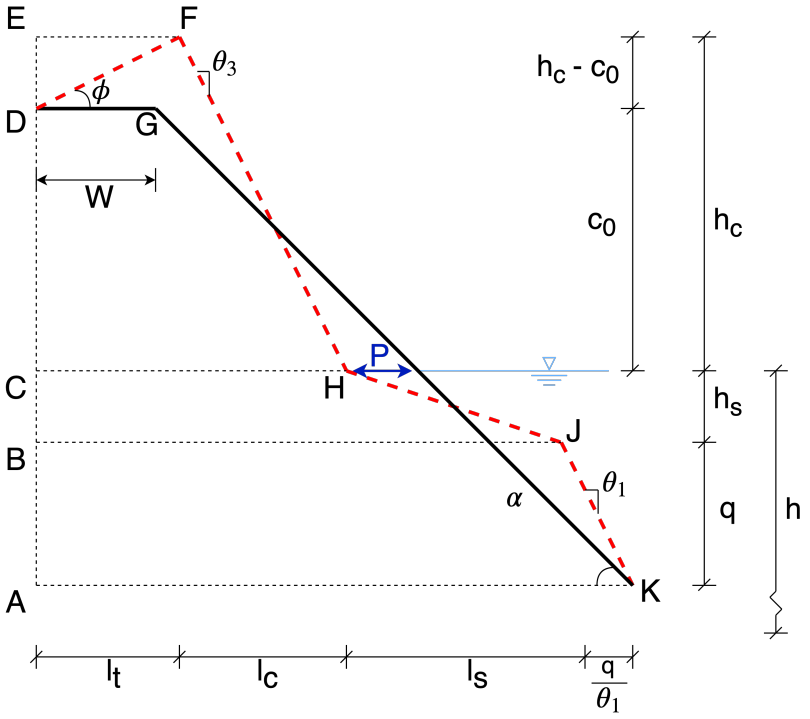

Figure 5.4: Schematic overview of the reshaping. The original profile is represented by the thick black line (DGK), the reshaped profile by the dotted red line. The blue arrow shows the horizontal translation of the local origin (H).

To solve p, fist the value for q is being computed.

To solve the mass balance, the initial profile (ADGK) needs to be equal to the reshaped profile.

$$A_{origin} = \left(q + h_s + c_0\right)\left(l_t + l_c + l_s + \frac{q}{\Theta_1} - \frac{q + h_s + c_0}{2\tan\alpha}\right) \tag{5.19}$$

The area of the reshaped profile (ABJK + BCHJ + CEFH - DEF) is:

$$A_{reshape} = q\left(l_t + l_c + l_s + \frac{q}{2\Theta_1}\right) + hs\left(l_t + l_c + l_s/2\right) + h_c\left(l_t + l_c/2\right) - \left(h_c - c_0\right)l_t/2 \tag{5.20}$$

To simplify the formulas, define:

$$A_0 = hs\left(l_t + l_c + l_s/2\right) + h_c\left(l_t + l_c/2\right) - \left(h_c - c_0\right)l_t/2 \tag{5.21}$$

$$L = l_t + l_c + l_s \tag{5.22}$$

Now equalizing both profiles to each other gives:

$$\left(q + h_s + c_0\right)\left(L + \frac{q}{\Theta_1} - \frac{q + h_s + c_0}{2\tan\alpha}\right) = A_0 + q\left(L + \frac{q}{2\Theta_1}\right) \tag{5.23}$$

Rewriting this in respect to q gives the parabolic function:

$$q^2\left(\frac{1}{2\Theta_1}-\frac{1}{2\tan\alpha}\right)+q\left(h_s+c_0\right)\left(\frac{1}{\Theta_1}-\frac{1}{\tan\alpha}\right)+\left(h_s+c_0\right)\left(L-\frac{h_s+c_0}{2\tan\alpha}\right)-A_0=0 \tag{5.24}$$

Using the ABC formula q can be computed. Subsequently the horizontal shift p of the local origin follows from:

$$p=q\left(\frac{1}{\Theta_1}-\frac{1}{\tan\alpha}\right)+l_s-\frac{h_s}{\tan\alpha} \tag{5.25}$$

With the formula of the horizontal shift of the local origin known, the reliability function can be composed. During the construction, up to a small amount of horizontal shift of the local origin (reshaping) is acceptable, as reshaped material can be put back in place with an excavator before placement of the underlayer. The damage threshold parameter (D_t) is introduced to define the maximum acceptable amount of horizontal shift. Horizontal shifts of P larger than this D_t is considered a damage event. After consulting with colleagues within Van Oord, the maximum acceptable shift D_t of P is set to 5 times the (D_{n50}). Resulting in the following reliability function:

$$Z=p-5D_{n50}=q\left(\frac{1}{\Theta_1}-\frac{1}{\tan\alpha}\right)+l_s-\frac{h_s}{\tan\alpha}-5D_{n50} \tag{5.26}$$

An important note is that different reshaping situations are possible, which also require slightly other calculations for q and p. All solutions are given in appendix D.

5.3.3. Damage calculation

With the reshaped profile known, the amount of damage follows from the area of erosion. This is the red area shown in fig. 5.5. After calculating the intersection points I_1 and I_2 between the original- and reshaped profile, the eroded area follows from:

$$Ae=0.5c_0I_{2,x}+(c_0-I_{1,y})I_{1,x}-0.5I_{1,x}I_{1,y}-0.5(I_{1,x}-G_x)(c_0-I_{1,y}) \tag{5.27}$$

Next the volume of the eroded material can be computed by multiplying it with the length of the open front.

$$V_{e,ce}=A_eL_{of,ce} \tag{5.28}$$

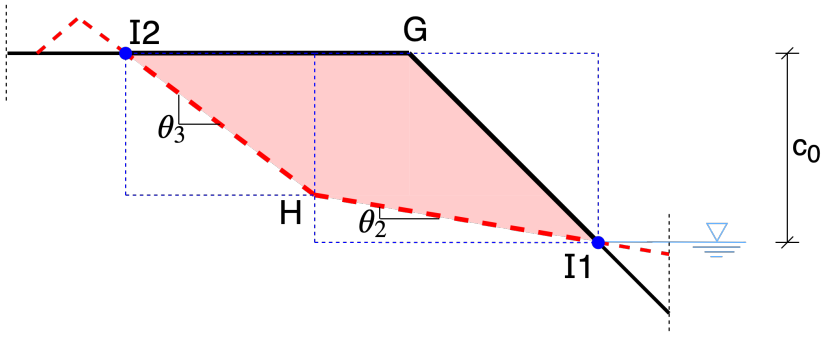

Figure 5.5: After reshaping the amount of damage is the eroded area (shown in red), between the initial profile (solid black line) and the reshaped profile (red dotted line)

5.3.4. Solutions for limitations

Core erosion larger than crest length

The method is limited by the length of the crest, as it is only valid for situations where crest recession is smaller than the crest width (see fig. 5.6a). As soon point D from fig. 5.4 reaches the rear slope, the mass balance is no longer valid (see fig. 5.6b). Both van der Meer and Merli did not fit the formulas for situations where the material was deposited on the rear slope of the structure. It may result in a severe underestimation of the damage when the maximum amount of reshaping is limited to the end of the crest.

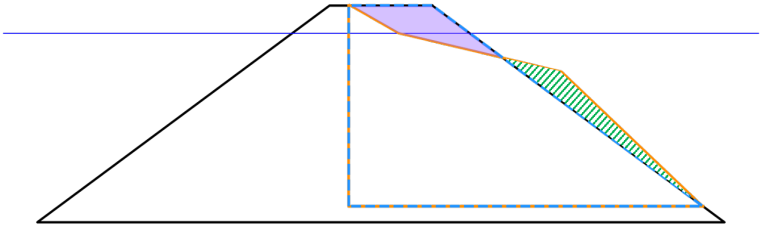

(a) Crest recession is smaller than the crest width, hence the mass balance is valid.

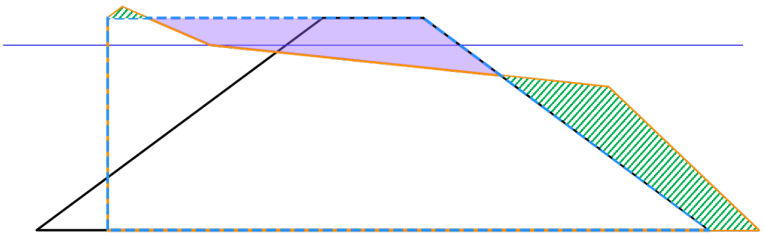

(b) Crest recession is larger than the crest width, hence the mass balance is invalid.

Figure 5.6: Two situations of calculation the reshaping of the emerged core. The mass balance is between the solid purple area and the striped green area. The solid purple shows the eroded material, and striped green shows the deposited material.

Proposed method

For estimating the amount of erosion, the following method is introduced. By considering the crest to have an infinite width, it is still valid to apply the mass balance. With the reshaped profile, the amount of damage is calculated the same as done in section 5.3.3.

By assuming an infinite wide crest, the reshaping will eventually tend towards a more or less equilibrium profile, which can be compared with the equilibrium profile of a beach. In the real situation, such an equilibrium profile can not develop, as the material deposits on the rear slope.

In fig. 5.7 the calculated damage is compared with lab experiments of Merli (2009) were the crest recession was larger than the crest width. Although the formulas are not intended for this situation, it closely follows the actual reshaped profile. Only at the end of the crest, the actual deformation becomes larger than the formulas predict. The predicted area of erosion is therefore slightly smaller than the actual area of erosion.

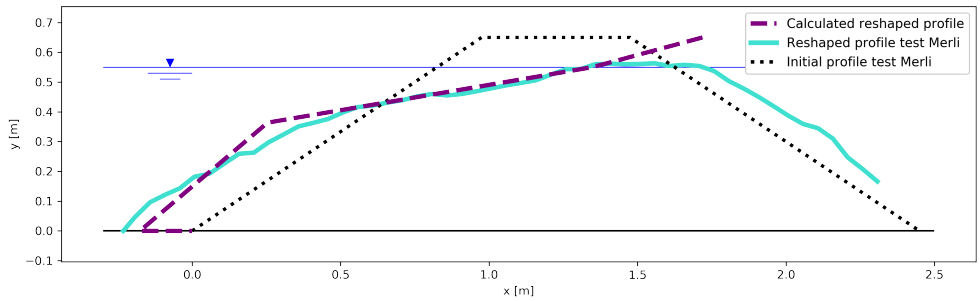

Figure 5.7: Comparison between the predicted reshaping according to the proposed method and the reshaped profile of physical test 7 from Merli (2009). The dotted purple line shows the reshaped profile according to the proposed method, and the thick light blue line the reshaped profile of the physical test.

Table 5.2: Input parameters of test 7 performed by Merli (2009).

ρ_s[kg/m^3]	Δ[−]	D_{n50} [m]	D_{85}/D_{15} [-]	H_s [m]	T_m [s]	N [-]
2659	1659	0.01102	17.7	0.1060	1.436	3000

The flume had a width of 0.8 m.

Core erosion after breaching underlayer

As mentioned in section 5.2.3, waves will start to erode the core as soon the underlayer is breached. Subsequently, underlayer material on top of the eroded core becomes unstable and will collapse into the eroded area leading to the mixing of the two construction materials. The influence of this process on the reshaping speed and profile is not known. No research has been done on the deformation of the underlying layers when the armour layer was (partially) eroded. Probably this was not considered relevant, as the structure already failed, regarding the research objective of protecting the underlying materials.

Proposed method

The situation is simplified by assuming the core will reshape the same as it would do without the underlayer on top of it, starting from the moment the underlayer is breached. Now the amount of damage to the underlayer can be calculated by the following method. The amount of waves needed the breach through the underlayer is calculated by rewriting equations 5.1, 5.2, 5.6 and 5.7 to a function for N. For eq. (5.1) (plunging waves in deep water) this is done below, the other three formulas are found in appendix D.

$$N_{exposure,pld} = \left[S_d \left(\frac{H_s}{\Delta c_{pl} P^{0.18} D_{n50} \xi_m^{-0.5}} \right)^{-5} \right]^2 \tag{5.29}$$

where:

S_d = is set to 8 (for a slope of 1:1.5)

Next, the amount of waves is subtracted from the total amount of waves during the storm. The remaining number of waves are then used to calculate the amount of reshaping of the core, according to the method described in section 5.3.4.

Since no physical model tests are executed for this situation, the only option to validate the proposed solution is to apply the method on the reference project. The storm of the reference project had a significant wave height of 4.97m and a mean period of 7.85s. In the model the storm had a total number of waves of 3000, as most of the reshaping has taken place after 1000 - 3000 waves (Van der Meer, 1988). It took 150 waves to breach through the underlayer, with the remaining 2850 the reshaping of the core is computed. In fig. 5.8, the reshaped profile obtained by the proposed solution is compared with the actual reshaped profile of the reference project after the storm. The profiles overlap quite well, hence supporting the proposed solution.

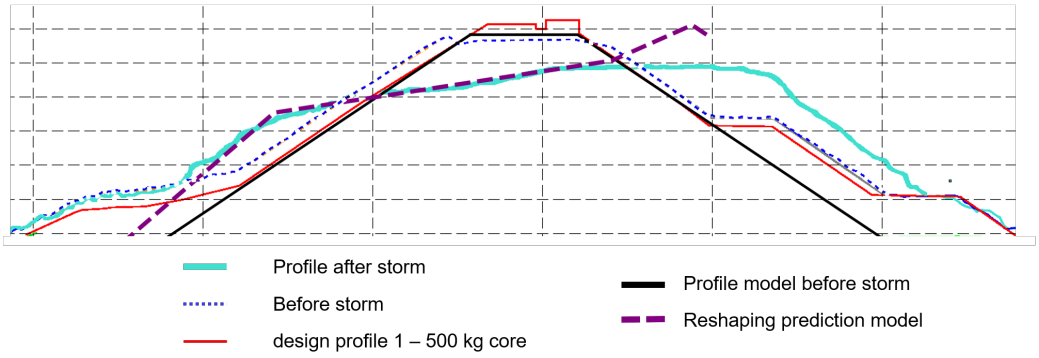

Figure 5.8: Comparison between the predicted reshaping according to the proposed method and the actual reshaped post-storm profile of the reference case (Van Oord, 2014). The dotted purple line shows the reshaped profile according to the proposed method, and the thick light blue line the reshaped profile of the reference case.

5.3.5. Process overview

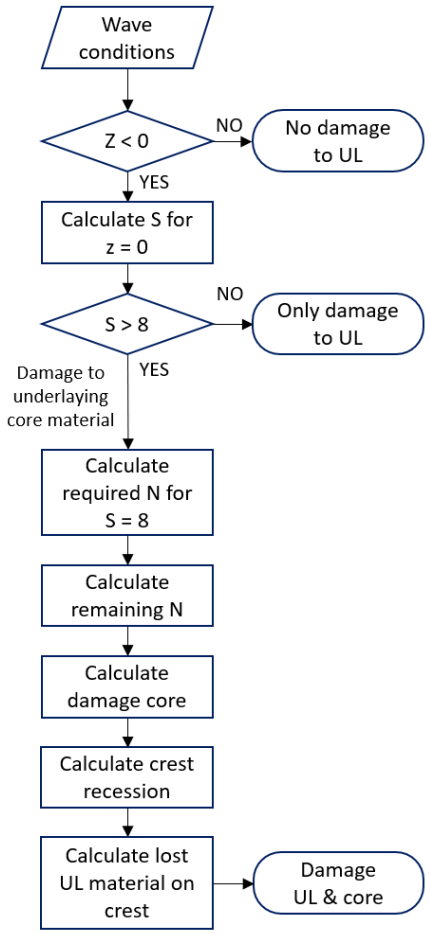

Figure 5.9: Flowchart of the process to define and quantify the damage for the breakwater section consisting of core and underlayer.

5.4. Submerged Core section

5.4.1. Literature

The submerged core section can be seen as a submerged breakwater (reef type breakwater), or a near-bed structure, prone to reshaping due to wave attack.

Analysing the literature for statically stable reef breakwaters, neither Vidal et al. (1995), Powell and Allsop (1985), Vidal et al. (2000) cannot be applied for the submerged core section. As most of the reference project parameters are far outside the validity ranges, all formulas result in unrealistic values.

For the dynamically stable submerged breakwater, Ahrens (1987) and van der Meer (1990) concentrated on the change in crest level due to wave attack. In appendix C.2, an explanation is found on why the literature on dynamically stable submerged breakwaters is not usable. The literature for near-bed structures, on the other hand, can be used. Vidal et al. (1995)

Near bed structures

Near-bed structures are described as submerged structures where the crest is relatively low, such that no severe wave breaking occurs due to this structure. Common near-bed structures are pipeline- and cable protection, underwater groynes and intake and outfall structures near power and desalination plants. However, the submerged core of a rubble mound breakwater can also be seen as a near-bed structure. In fig. 5.10, a sketch of a near-bed structure and the corresponding most important parameters are shown.

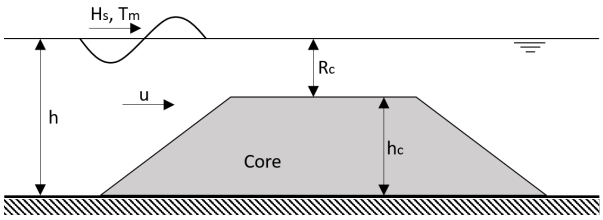

Figure 5.10: Overview sketch of a near-bed structure, based on Wallast and van Gent (2002)

Wallast and van Gent (2001) studied submerged rubble mound structures with a relatively low crest, such that wave breaking does not have a significant influence. They performed physical model tests to investigate the stability of near-bed structures under wave attack and currents. A JONSWAP spectrum was used to describe irregular waves. Based on the created data and the analysis of existing data (Lomónaco, 1994), several methods to predict the stability where analysed. They that the velocity-based mobility parameter (Θ), was the most appropriate method to describe the damage.

$$\Theta = \frac{u^2}{g\Delta D_{n50}} \tag{5.30}$$

Here u is the local characteristic velocity [m/s]. For this local characteristic velocity, the peak bottom velocity is used as it would be the velocity at the crest of the near-bed structure. The equation below gives the maximum wave-induced orbital velocity (m/s), based on the linear wave theory.

$$u = \hat{u}_0 = \frac{\pi H_s}{T_m} \frac{1}{\sinh k h_c} \tag{5.31}$$

The damage development can now be computed with the founded relationship between the damage level parameter S:

$$\frac{S}{\sqrt{N}} = 0.2\Theta^3 = 0.2\left(\frac{u^2}{g\Delta D_{n50}}\right)^3 \tag{5.32}$$

In the equation above, no parameter describes the influence of currents. Although there is an influence of currents on the amount of damage, available data shows that this influence is neglectable for the following range: $U/u_0 < .2$, in which U is the depth-averaged current velocity (m/s), and for the following range of the mobility parameter: $0.15 < u_0^2/(gD_{n50}) < 3.5$ (Wallast and van Gent, 2001). Outside this range, more research would be necessary, as neglecting the effects of currents for conditions outside the range of the present dataset cannot be justified based on the analysis by Wallast and van Gent (2001). For the the case situation, scenarios are possible where $u_0^2 = (gD_{n50}) > 3.5$, which can occur during large storms. This would imply to take currents into account. As the hydraulic system of the case project is not known for having strong currents, the formula is considered valid to use. No other known literature describes the situation.

5.4.2. Reliability functions

In formula eq. (5.32), the nominal stone diameter (D_{n50}) is seen as the resistance (R). The load is defined as the local characteristic velocity (u) multiplied/divided by the remaining parameters in the formula. This results in the following reliability formulas:

$$Z = D_{n50} - \left(\frac{0.2u^2\sqrt{N}^{1/3}}{g\Delta(S_d)^{1/3}}\right) \tag{5.33}$$

5.4.3. Damage calculation

For calculating the amount of damage, the actual damage number is required. The actual damage number can be obtained by rewriting eq. (5.33) as a formula for S and set Z equal to zero, resulting in the following formula:

$$S = 0.2\left(\frac{u^2}{g\Delta D_{n50}}\right)^3\sqrt{N} \tag{5.34}$$

With S known, the eroded area is obtained the same way as eq. (5.14):

$$A_e = SD_{n50}^2 \tag{5.35}$$

By multiplying the eroded area with the length of the open section of the submerged core, the total volume of the eroded core material is calculated:

$$V_{e,ucs} = A_e L_{of,cs} \tag{5.36}$$

Where:

$V_{e,cs}$	=	Volume of the eroded material	[m^3]
$L_{of,cs}$	=	Length of the open front of the submerged core	[m]

5.4.4. Limitations

Applying the method on the reference case, the only parameter that may be outside the validity range of the formulas is the ratio wave height – depth at crest (H_s/R_c [-]).

Table 5.3: Validity range of eq. (5.31) and eq. (5.32).

Parameter	Symbol	Range
Front side slope (-)	$tan\alpha$	1:8 – 1:1
Relative buoyant density (-)	Δ	1.45 – 1.7
Number of waves (-)	N	1000 – 3000
Fictitious wave steepness (-)	$s_o m$	0.03 – 0.07
Non-dimensional velocity (-)	$U^2/(g\Delta D_{n50})$	0 – 10
Ratio wave height – water depth (-)	H_s/h	0.15 – 0.5
Ratio wave height – depth at crest (-)	H_s/R_c	0.2 – 0.9
Stability number (-)	$H_s/(\Delta D_{n50})$	5 – 50
Damage level parameter (-)	S_d	< 1000

Applying the method on the reference case, the only parameter that may be outside the validity range of the formulas is the ratio wave height – depth at crest (H_s/R_c [-]).

When formula is tested with the case situation (core level at -6 cd) for an storm event with H_s = 5.0 m and T_m = 8 s, the damage according to eq. (5.35) is almost as large as the cross-sectional area of the submerged core. Following from expert judgement, this is considered too much.

Proposed solution

The largest value within the validity range of the ratio wave height/depth at the crest (H_s/R_c) is 0.9. Using the Hs, and dividing it by 0.9, the largest possible crest height within the validity range can be determined. Using the significant wave height and the validity range of the relative freeboard, the largest crest height within the validity range can be determined (see fig. 5.12). This maximum valid crest height ($h_{c,max\ valid}$), is used to calculate the post-storm crest height. Now the total erosion becomes the area between the initial actual crest height and the post-storm crest height, calculated with the $h_{c,max\ valid}$ (see fig. 5.13).

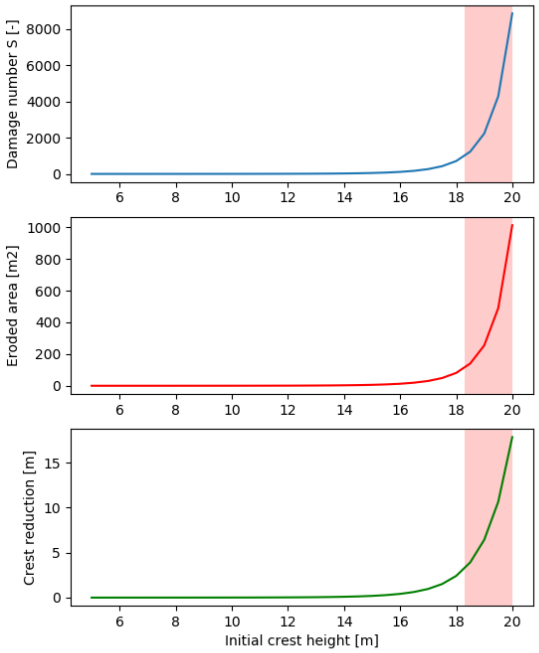

Figure 5.11: The relation between the initial crest height and the damage number (S) (top graph), eroded area (Ae) (middle graph), and the crest reduction after the storm (lower graph), for the case situation. The red area indicates where the use of the formula is not valid anymore, as the situation is outside the validity range.

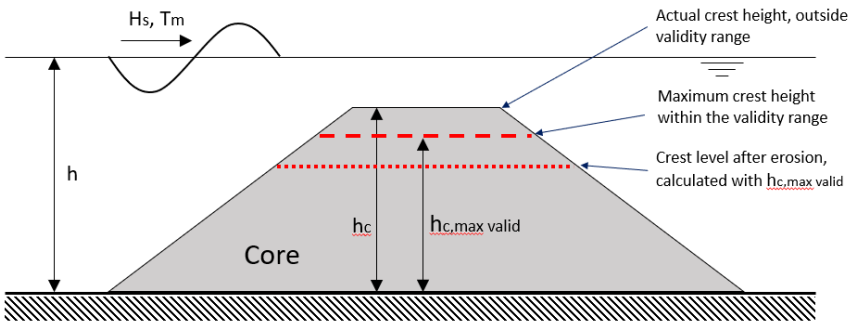

Figure 5.12: Cross-sectional profile of the submerged core section, where the crest height is outside the validity range of formula, given the wave height. The red striped line shows the largest crest height within the validity range, given the wave height. This maximum valid crest height is then used to calculate the crest level after erosion (the red dashed line).

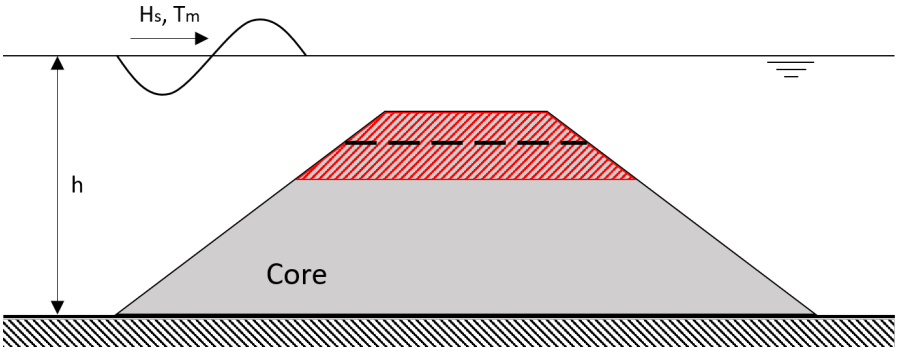

Figure 5.13: Cross-sectional profile of the submerged core section, with the area of erosion (showed as the red striped area). The total erosion consists of the area between the actual crest height and the maximum crest height in the validity range (area above the striped black line), and the area of erosion computed using the maximum crest height in the validity range (area below striped black line).

No data of the reference project is available to validate this proposed method for the damage estimation. At the time the reference project was damaged due to the storm, the core sections where already finished and the breakwater only consisted an open front of the underlayer.

6

Hydraulic boundary conditions

The model uses a dynamic stochastic fixed time step simulation. The model checks per time-step if the randomly sampled least favourable conditions result in damage, as the least favourable condition per time step is decisive for the occurrence of damage. This least favourable condition is randomly sampled from the joint probability distribution function of the weekly maxima. This function is obtained from hindcast pairs of wave height and wave period. In particular, available data is used to arrive at a distribution function for the wave height by applying the block maxima approach. Subsequently, a parametrized relation between wave height and wave period is obtained from the time series to find a distribution function for the wave period given some wave height. It would also be possible to switch this relation and let the wave height depend on the wave period. However, it is generally assumed that the wave height is the dominant parameter. Hence it is decided to sample the wave height directly from the obtained distribution functions.

As described in section 3.2, the return period of a particular hydraulic event is not stationary over the year. To include the non-stationary behaviour of the wave climate, the distribution function for the wave height and period will be obtained for each meteorological season, instead of the entire year. So the 16-year time series need some preparation in order to end up with a data set of weekly maximum wave heights for each season. Section 6.1 outlines the preparation of the offshore time series. Next, in section 6.2, the distribution functions representing the weekly maximum wave height are obtained by using the block maxima method. In section 6.3, the parametrized relation between the wave period and wave height is obtained and used to find the distribution function for the mean wave period. Section 6.4 describes what is done with the storm surge and tidal range, and section 6.5 ends the chapter by providing an overview of the sampling process.

6.1. Data preparation

First, the data is separated into independent peaks. Secondly, the weekly maximum wave height is selected per week for the 16-year time series. The last step is to separate the weekly maximum wave heights over the four seasons.

6.1.1. Independent peaks

The 16 years time series of offshore wave data was computed with a 6 hour time interval. In order to apply the block maxima method on this time series, it is essential to separate the data in independent peaks. This prevents other high wave heights around the peak value are included in the analyses.

The discrete offshore time series is scanned for peaks, and the independent ones are collected in a new dataset. An element of the time series is considered a peak if it is not smaller than its two direct neighbours and larger than at least one of them. Peaks are considered independent if they are at least w hours apart in the time series (see fig. 6.1a). In this study, w depends on the magnitude of the highest of the neighbouring peaks (see fig. 6.1b). If the peak is less than w hours apart, it is considered the same storm event as the higher peak.

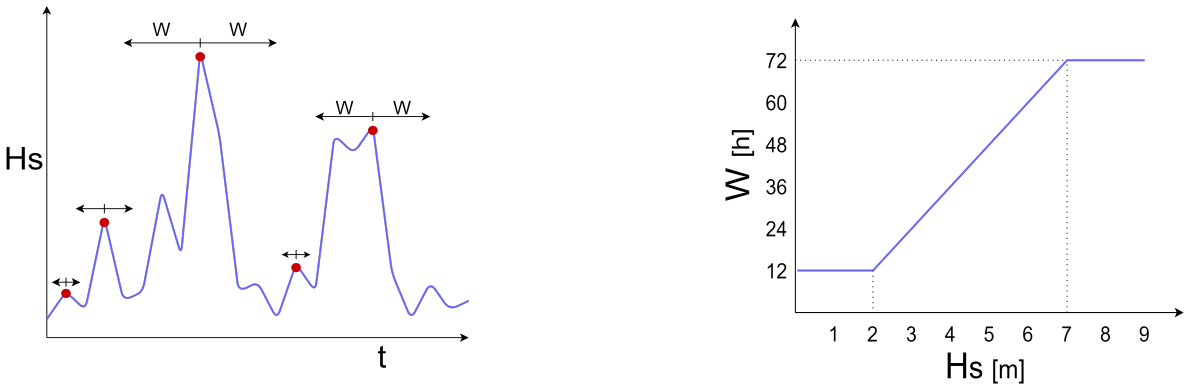

(a) The peak is considered independent if it is at least w hours away from a higher peak. The red dots indicate an independent peak.

(b) The relation between the wave height and the amount of separation w.

Figure 6.1: Independent peak selection method

In appendix ... more insight in the method used to select the independent peaks can be found.

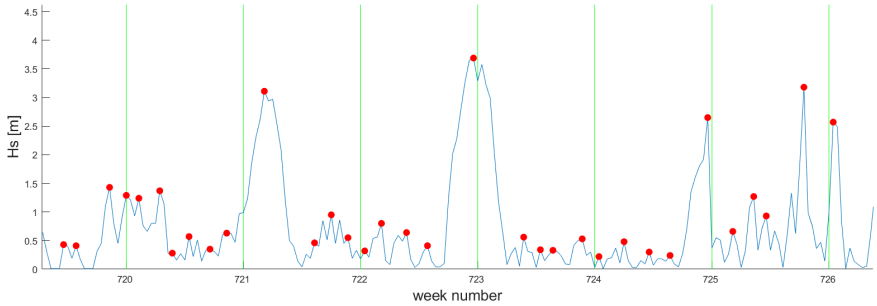

Figure 6.2: Identification of independent peak events (red dots), such that the same storm can never be counted by two different weeks as the highest wave height. The weeks are separated by the green vertical lines.

The result of selecting the independent peaks can be seen in fig. 6.2. With all the dependent peaks filtered out of the dataset, the maximum wave height per week can be selected. The 16-year time series contains 5902 days, with each four measures per day. Per seven days, the maximum wave height is selected and together with its corresponding values for the other hydraulic conditions stored in a new data set. Now the new data set contains 844 weekly maximum wave heights, with the corresponding wave period and the actual date the peak was measured. Dividing the time series in equal sized bins, and selecting the highest value, corresponds with the block maxima method. More on the block max method is covered in section 6.2.

6.1.2. Seasonality

To include the effect of seasonality, one option is into separate the data in seasons and then analyse the data per season (Carter and Challenor, 1981). Another option is to make the parameters of the extreme value distribution function time-dependent (Menéndez et al., 2009). For this study, the first option is selected, as it is considered more pragmatic. The 844 weekly maximum wave heights are divided over four meteorological seasons:

- Winter (Dec, Jan, Feb)
- Spring (Mar, Apr, May)
- Summer (Jun, Jul, Aug)
- Autumn (Sep, Okt, Nov)

Hence each season contains 16 times three months of data. The month in with the weekly maximum wave height is measured, determines in which season this value is allocated. By using this method to divide the

measurements over the seasons, may result in a slight difference in number of data points between the seasons.

The four obtained data sets with the weekly maximum wave heights are used in the next two sections (6.2 & 6.3) to find the distribution functions for the wave height and period. In fig. 6.3 the histograms of the weekly maximum wave heights are shown for each season.

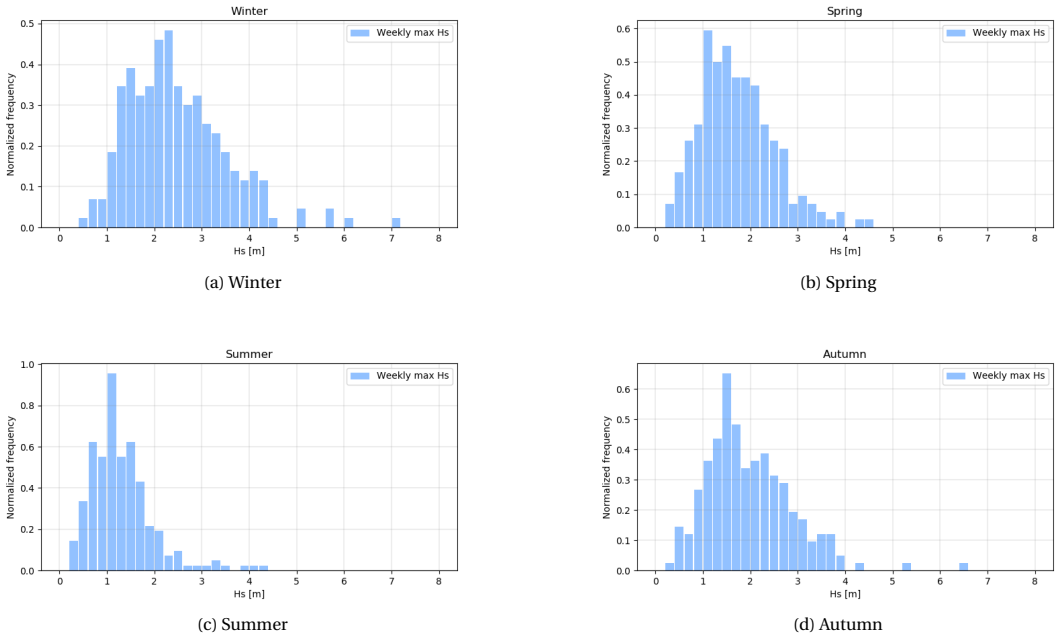

(a) Winter

(b) Spring

(c) Summer

(d) Autumn

Figure 6.3: Histograms of the weekly maximum wave height for each season.

6.2. Distribution functions wave height

The extreme value theory (EVT) is used to describe the weekly extremes.

6.2.1. Method

The block maxima method in ETV consists of dividing the time series into non-overlapping periods or blocks of equal size and focus attention to the maximum observation in each period. These observations follow an extreme value distribution. A goodness of fit is applied to find the distribution function and its corresponding parameters that fit the data best.

According to For the analysis, the following extreme distribution functions are analysed:

- Generalized extreem value distribution
- Gumbel distribution
- Weibull distribution

Fitting of the theoretical distribution functions to the seasonal data is done in Python, and the function stats.<distribution>.fit is used to find the parameters of the distribution functions.

The fitted distribution functions for the spring season are shown in figure 6.4 together with the data. In appendix E, the fitted distribution function, together with the empirical data, is shown for the other seasons.

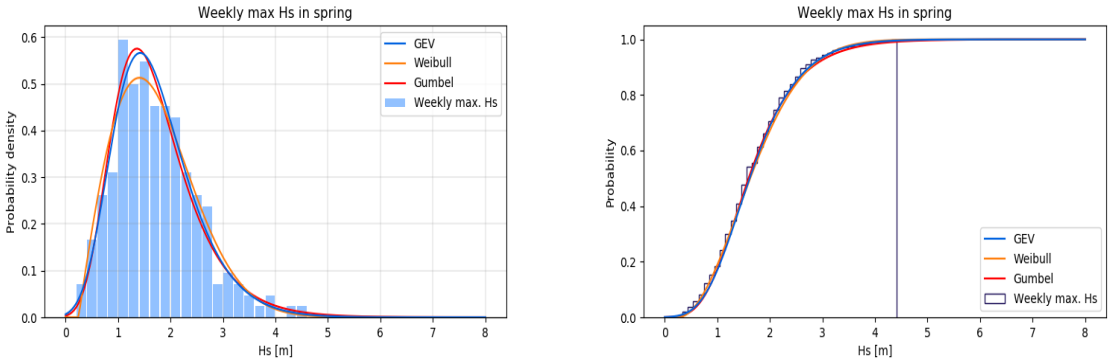

(a) Histogram of the weekly maximum wave heights in spring and the three fitted theoretical probability density functions.

(b) Cumulative distribution of the weekly maximum wave heights in spring and the three fitted theoretical cumulative distribution functions.

Figure 6.4: The histogram and cumulative distribution of the weekly maximum wave heights in spring (from time series), compared with the fitted theoretical probability density functions and cumulative distribution functions.

6.2.2. Results

A goodness of fit is used to find the best fitting distribution function. The sum of squared difference is selected as the goodness of fit, and its results are shown in table 6.1.

Table 6.1: Results from the goodness of fit

Data	Sum of squared difference		
	GEV	Gumbel	Weibull
Weekly max winter	2.835	9.5121	4.3871
Weekly max spring	2.5004	8.7422	3.3698
Weekly max summer	3.0432	8.8127	3.8487
Weekly max autumn	3.1284	9.3243	4.0443

From table 6.1 follows that the generalized extreme value distribution represents the weekly maximum wave height for all seasons best. The cumulative distribution function is described by:

$$F(x) = \begin{cases} \exp\left(-\left[1+\xi\dfrac{x-\mu}{\sigma}\right]^{-1/\xi}\right) & \text{if } \xi \neq 0 \\ \exp\left(-\exp\left[-\dfrac{x-\mu}{\sigma}\right]\right) & \text{if } \xi = 0 \end{cases} \tag{6.1}$$

Here μ is the location parameter, σ is the scale parameter and ξ is the shape parameter. Together they form the distribution parameters. In table 6.2 the distribution parameters of the fitted generalised extreme value distributions are shown.

.

Table 6.2: Distribution functions

Data Set	Variable	Distribution	Parameter estimates
Weekly maxima winter	H_s	Generalized extreme value	μ = 2.002742 σ = 0.829367 ξ = 0.013835
Weekly maxima spring	H_s	Generalized extreme value	μ = 1.381519 σ = 0.650813 ξ = 0.061868
Weekly max summer	H_s	Generalized extreme value	μ = 1.005646 σ = 0.479515 ξ = -0.048646
Weekly max autumn	H_s	Generalized extreme value	μ = 1.569033 σ = 0.735234 ξ = 0.027008

With the found theoretical distribution function for each season, the model can randomly sample significant wave heights, which represents the actual situation. In the next section, the relation between Hs and Tm is lined out, and a method is introduced to sample the wave period, given a certain wave height.

6.3. Distribution function wave period

As the model will randomly sample a value for H_s per time step, and due to the dependence between H_s and T_m, it is not possible to obtain the wave period from a separate distribution function. In chapter 4, it is already mentioned that the location of the reference project is characterised by wind sea conditions; swell conditions do not occur. Wind waves are characterised by the strong correlation between the wave height and the wave period. It turns out that the correlation between the wave height and period of the 16-year time series is almost the same as the correlations for the seasonal data; hence it is not required to find four different relations between the H_s and T_m (one for each season). Instead, one relation will be obtained using the weekly maximum data of all seasons together. In fig. 6.5 the correlation between the weekly maximum significant wave height and the corresponding mean wave period is shown, using the weekly maximum time series (H_i, T_i)(with $i = 1...844$).

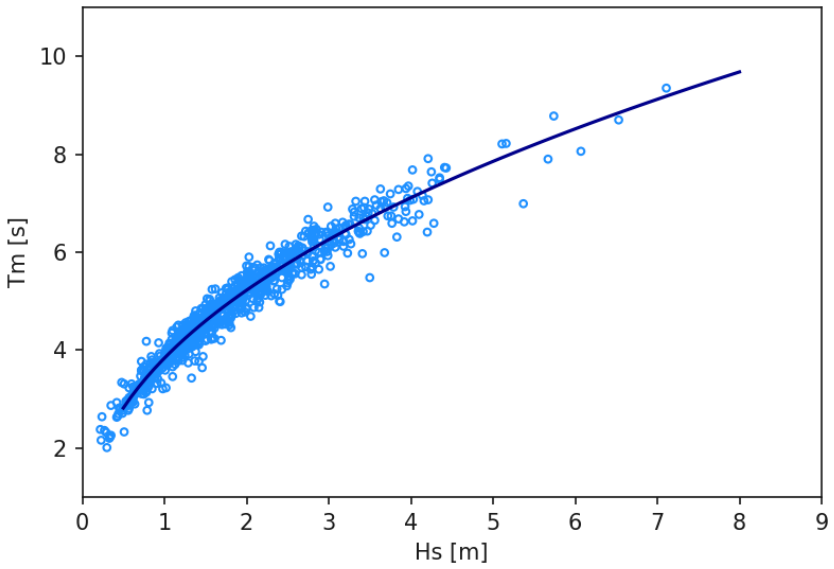

Figure 6.5: Scatter between the observed weekly maximum wave height and the corresponding mean wave period.

By using linear regression the following trendline between H_s and T_m is obtained and shown in fig. 6.5:

$$T_m = 3.8366 H_s^{0.4389}$$

Using this trendline with the random sampled value for H_s, a corresponding value for T_m can be obtained. However, as can be seen in fig. 6.5, there is a natural spreading of the wave period around the trend line. To obtain this spreading of the wave period, the time series could be parametrized by describing the period T as a normally distributed variable:

$$\hat{T} \sim N(\mu, \sigma) \tag{6.2}$$

The ˆ stands for parameterized, where the mean (μ) and standard deviation (σ) depend on the wave height H:

$$\mu = \beta H^{\alpha} \tag{6.3}$$

$$\sigma = p H^{\alpha} \tag{6.4}$$

It follows from the trendline, that $\beta = 3.8366$ and $\alpha = 0.4389$. By selecting the mean and the standard deviation such, that they both depend on the wave height in a corresponding way, a scaling of the period can be applied. Combining eq. (6.2), eq. (6.3) and eq. (6.4) lead to:

$$\frac{\hat{T}}{\beta H^{\alpha}} \sim N(1, \frac{p}{\beta}) \tag{6.5}$$

Due to the scaling of the period, the standard deviation now becomes a constant. For conveniance the scaled period is defined as Y:

$$Y_i = \frac{T_i}{\beta H_i^{\alpha}} \tag{6.6}$$

The variance of Y than becomes:

$$s^2 = \frac{1}{n} \sum_{i=1}^{n} (Y_i - Y_{mean})^2 \tag{6.7}$$

where:

$$Y_{mean} = \frac{1}{n} \sum_{i=1}^{n} Y_i \tag{6.8}$$

Now p follows from:

$$p = \beta s \tag{6.9}$$

With the values for α and β the values for Y and its corresponding variance s^2 are calculated, resulting in a $S^2 = 0.0028$ and $s = 0.0528$. From eq. (6.9) follow $p = \beta s = 0.2025$.

Now with the value of the wave height known, a random wave period can be sampled form the following distribution function, such that it represents the data:

$$\hat{T} \sim N\Big(3.8366 H^{0.4389},\ 0.2025 H^{0.4389}\Big) \tag{6.10}$$

In fig. 6.6 the scatter between the significant wave height and the mean period of the empirical data and of the randomly generated data is shown. First the wave height is randomly sampled from the found distribution functions in section 6.2, secondly a value for the wave period is sampled from eq. (6.10), given the value for H_s. The generated data, shows a good fit with the empirical data. For wave heights smaller than 1 m, the

accuracy between the wave height from the time series and the sampled wave heights decreases, however as these wave will not result in damage it is of no issue for the research objective.

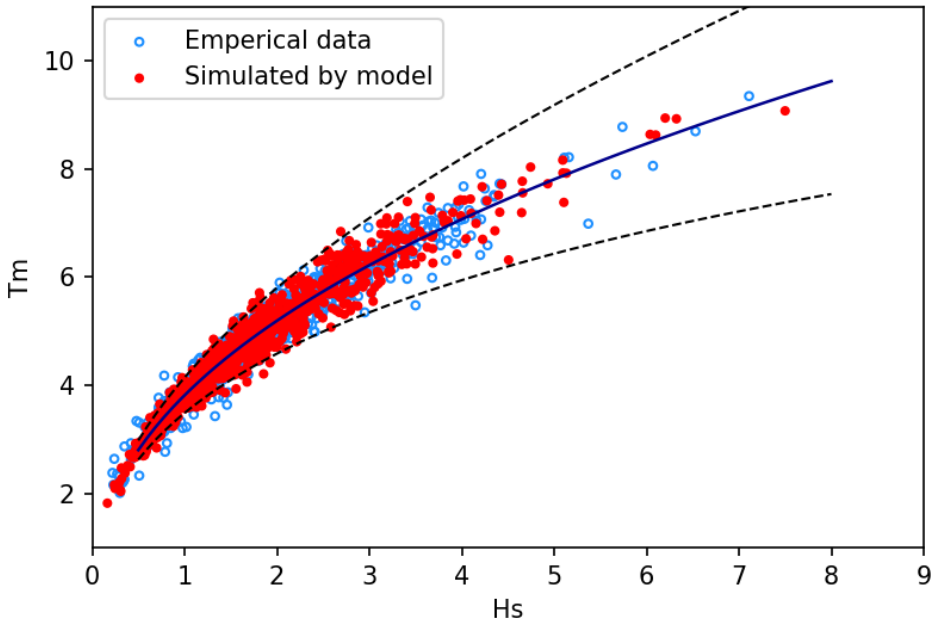

Figure 6.6: Scatter between the weekly maximum wave height and the corresponding mean wave period of the time series (givin in blue open dots), and the random sampled weekly maximum wave height and the corresponding mean wave period by the model (solid red dots). The black dashed line indicates the 90% confidence interval.

6.4. Water levels

The 16-year time series does not include measured water levels. According to the design wave conditions report (Van Oord, 2013), the maximum storm surge is +0.96 m, compared to the water depth of 25 m this is very small. Furthermore, the difference between storm surge of a 1/1 year storm event and a 1/50 year storm event is only 0.2 m. As the water level is missing in the 16-year time series and the surge is relatively small compared to the water depth in the situation of the reference case, the storm surge is not included for the reference case.

The area has a tidal range of 0.06 m (Van Oord, 2013). Compared to a water depth of 25 m, a tidal range that small is considered negligible, and not included in the model.

6.5. Sampling process

With the required distribution functions obtained from the data, the model can sample the hydraulic boundary conditions such it represents the data.

Per time step the model will check in which season the time step is. Depending on the season, the model will randomly sample a wave height from the seasonal cumulative distribution function.

The flowchart in fig. 6.7 shows the process needed for obtaining the distribution functions, which are used to random sample wave conditions that are representing the actual situation. This method can be used for other breakwater projects.

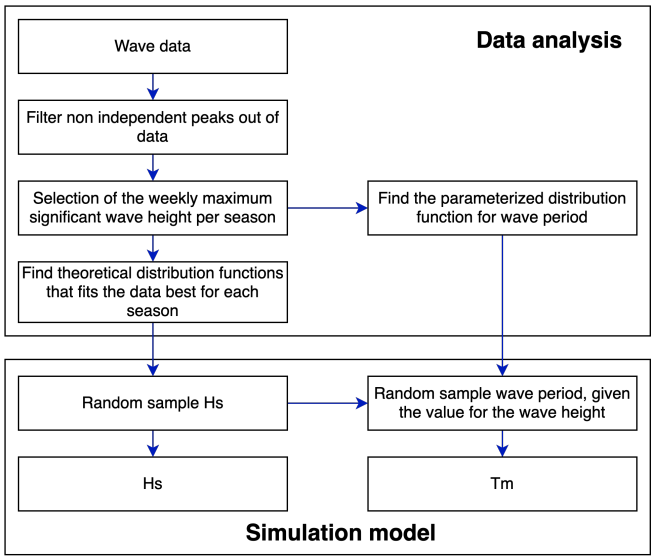

Figure 6.7: The flowchart shows the process needed for obtaining the theoretical distribution functions which represent the actual situation, and how these theoretical distribution functions are used in the simulation model

7

Repair works

The quantitative damage calculations introduced in chapter 5, express the damage in cubic meters of eroded material. This chapter lines out the method to determine the required repair time and to express the damage in euros.

7.1. Repair method

Like the construction works, the repair is carried out using land-based operations, marine-based operations or a combination of these two. Usually, land-based operations are applied wherever physically possible, as they are less expensive compared to marine-based operations.

Although preferred, it is not always possible to repair the damage only using land-based equipment. Due to reshaping, the crest width of the post-storm profile may be too small to allow land-based machinery, or material needs to be recovered from deep areas not accessible by land-based equipment (see fig. 7.2).

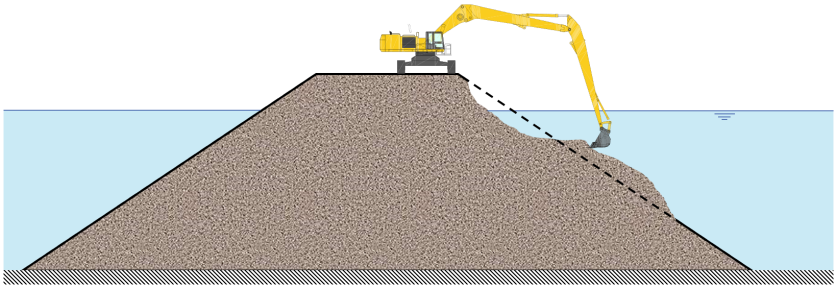

Figure 7.1: Land based repair works.

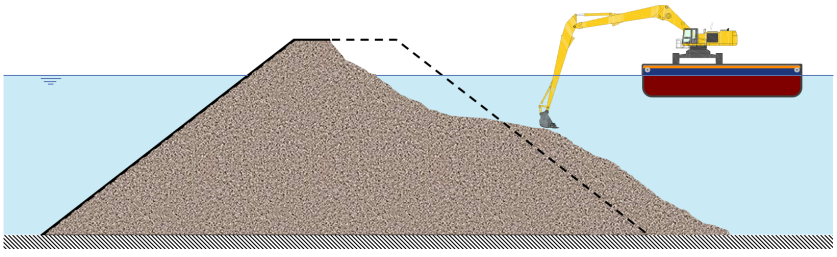

Figure 7.2: Marine based repair. Crest width too small for land-based equipment.

In other situations, the deposited material is simply out of reach for land-based equipment, this due to larges dimensions of the breakwater or deep water, see fig. 7.3. In practice, a combination of the two operations is mostly used.

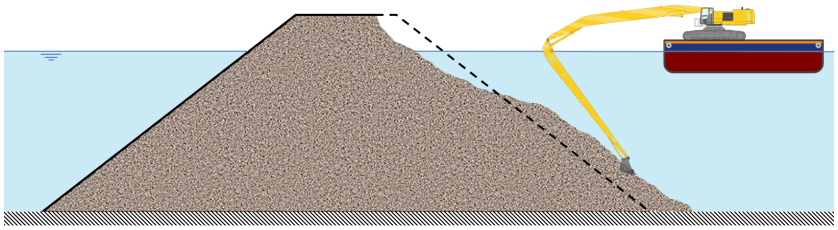

Figure 7.3: Marine based repair. Land-based equipment can not reach all the damage, due to a high crest level and/or a deposited material at deep levels.

Damage to the submerged core is repaired using marine-based equipment. For the underlayer- and emerged core section, it becomes quite challenging to predict what percentage of the damage is repaired by land-based operations and which by marine-operations. Without computing the best repair strategy, it is still possible to find a representative ratio between the two repair operations, using the same ratio between land- and marine-based operation from the construction phase, for the repair works.

For the reference case this leads to the following ratios between land-based and marine based repair (Van Oord, 2013):

Table 7.1: Ratia between land-based and marine repair operations.

Open front section	Part land-based operations	Part marine-based operations
Underlayer	1/3	2/3
Emerged core	1/3	2/3
Submerged	0	1

7.2. Repair calculations

7.2.1. Repair time calculations

Chapter 5 introduced the methods to calculate the volume of damage in m^3. In order to compute the time needed to repair the damage, the amount of damage is needed in tonnes. With the amount of damage known in tonnes, the required repair time can be obtained by dividing the damage by the repair capacity.

Repair capacities for a specific project are influenced by the contractor experience, weather exposure, available equipment on site, and whether repair work is land-based or marine-based (CIRIA; CUR; CETMEF, 2007). For the reference case the production rates for construction are shown in table 7.2.

Table 7.2: Building rate

Production		1 - 500 kg	1 - 3 ton
Landbased	ton/wk	32,000	18,000
Marine	ton/wk	30,000	15,000

The repair rates are estimated to be considerable lower than the construction rates (personal communication Van Oord). Based on expert judgement the repair rates are obtained by dividing the building capacity by three.

Table 7.3: Repair rate

Production		1 - 500 kg	1 - 3 ton
Landbased	ton/wk	10,666	6000
Marine	ton/wk	10,000	5000

As progress in the model is only possible if all the damage has been repaired, the total repair time depends on the section with the largest required repair time. However, as the submerged core and emerged core consist of the same material, they require the same type of machinery (de Pater, 2019). The required repair time for the emerged core section and the submerged core section are added together, as the same machinery is used. In the situation, the underlayer is breached, and core material of the underlayer section reshaped, the repair time of all sections need to be added together.

The total repair if the underlayer is not breached:

$$T_{repair} = \max\left(T_{repair,UL}\ ;\ \left(T_{repair,ce} + T_{repair,cs}\right)\right) \tag{7.1}$$

The total repair if the underlayer is breached:

$$T_{repair} = T_{repair,UL} + T_{repair,ce} + T_{repair,cs} \tag{7.2}$$

Where:

T_{repair}	=	Total repair time	[weeks]
$T_{repair,UL}$	=	repair time required for the underlayer (UL) section	[weeks]
$T_{repair,ce}$	=	repair time required for the emerged core (ce) section	[weeks]
$T_{repair,cs}$	=	repair time required for the submerged core (cs) section	[weeks]

Since the time steps size in the model is one week, the required repair time obtained needs to be rounded to an integer. For the cost calculations, the rounded number of weeks is used.

7.2.2. Damage costs calculations

With the required amount of weeks needed to repair the damage known, the corresponding cost due to the damage and required repair can be calculated. The cost consists of repair work and overhead cost. In the event the underlayer is breached, and mixing of material occurred, procurement of new underlayer material is needed. In table 7.4, an overview is given of all the costs related to the repair works.

Table 7.4: Costs corresponding with the repair. The costs are given in euro per week.

Cost variables		Rock classes	
		1-500 kg (core)	1-3 ton (underlayer)
Land based repair	€/ week	55,000	70,000
Marine based repair	€/ week	90,000	120,000
Overhead costs (staff etc)	€/ week	60,000	60,000
Rock procurement + transport	€/ ton	12	24

8

Sensitivity analysis

The reference case is used in the context of investigating the feasibility of a model, with which risks related to the construction phase of rubble mound breakwaters in sea-state conditions can be determined. Validation of the model, however, is not possible as not all required data is available for this study. The sensitivity analysis of the model and its parameters is not affected by this, and can still be performed. The sensitivity analysis examines the sensitivity of input parameters on the model output, which is needed to answer the fourth research question introduced in section 1.3. A distinction is made between the following input parameters:

1. Sensitivity of the starting date construction works.
2. Input parameters representing a magnitude, which can be influenced (introduced in section 8.3.1).
3. Formula parameters.

All three input parameter types will be analysed. Usually, the sensitivity of a parameter on the model output is expressed as the percentage change of the parameter vs the percentage change of the model output (Saltelli, 2008). As model output, the mean financial risk for the contractor and the mean financial risk for the insurance company are selected. Since this can not be applied for the sensitivity analysis of the start date, as there is no percentage change possible of a date, other methods will be used.

The reference case is used to obtain the model outputs for analysing the input parameter sensitivity. In section 8.1, the input parameters used for the reference case are discussed. Sections 8.2.1 describes the different scenarios for the starting date and their sensitivity result. Section 8.3 describes the examined input parameters, the different scenarios and their sensitivity result. In section 8.4 the same is done, but for the formula specific parameter. Section **??** ends the chapter with the conclusion.

8.1. Base case description

To analyse the sensitivity of parameters a base case is needed to compare the change in model output when varying input parameters. In this section, the input parameters used for obtaining the base case model output are described.

8.1.1. Input parameters base case

The construction of the reference case starts on the 3rd of march 2014. The nominal construction time is 30 weeks, in other words, if no delay takes place the breakwater sections are build in 30 weeks. Next the general input variable are shown in table A.1.

Table 8.1: General input variables

Variable	Symbol	Distribution	Mean μ	Standard deviation σ
Number of waves [-]	N	Normal	3000	200
Slope [°]	α	Normal	1.5	0.05
Gravitational acceleration [m/s^2]	g	Deterministic	9.81	-
Nominal diameter underlayer [m]	$D_{n50,ul}$	Normal	1.054	0.06
Nominal diameter core [m]	$D_{n50,c}$	Normal	0.338	0.03
Density of stone [kg/m^3]	ρ_s	Normal	2650	10
Density of water [kg/m^3]	ρ_w	Normal	1016	2
Lenght open front underlayer [m]	$L_{of,ul}$	Deterministic	100	-
Lenght open front emerged core [m]	$L_{of,ce}$	Deterministic	100	-
Lenght open front submerged core[m]	$L_{of,cs}$	Deterministic	100	-

Besides the general input parameters, there are also some parameters used only in a specific formula. The reliability function for the underlayer (eq. 5.8, 5.9, 5.10,5.11), emerged core (eq. (5.26)) and submerged core (eq. (5.33)) all have one or more formula specific input variable. In the following tables the values of these formula specific input variables are described.

Table 8.2: Formula specific input variables underlayer section

Variable	Symbol	Distribution	Mean μ	Standard deviation σ
Notional permeability [-]	P	Deterministic	0.4	-
Damage number [-]	S_d	Deterministic	2	-
Plunging coefficient, deep water [-]	$c_{pl,d}$	Normal	6.2	0.4
Surging coefficient, deep water [-]	$c_{s,d}$	Normal	1.0	0.08
Plunging coefficient, shallow water [-]	$c_{pl,s}$	Normal	8.4	0.7
Surging coefficient, shallow water [-]	$c_{s,s}$	Normal	1.3	0.15

Table 8.3: Formula specific input variables emerged core section

Variable	Symbol	Distribution	Mean μ	Standard deviation σ
Damage threshold [m]	D_t	Deterministic	5*$D_{n50,c}$	-

Table 8.4: Formula specific input variables submerged core section

Variable	Symbol	Distribution	Mean μ	Standard deviation σ
Damage number [-]	S_d	Deterministic	2	-

8.1.2. Number of simulations

Before the base case is analysed by the model, the number of simulations of the Monte Carlo has to be selected. The number of simulation in the Monte Carlo needs to be high enough, such that stable model output is generated. A stable model output means that the variation in output between multiple runs using the same input variable is marginal. To obtain the number of simulation required for a stable output, multiple runs are executed with the same number of simulations. The number of simulations is increased until they approach a more or less constant value for the model output. In this case, the mean financial risk is used as model output.

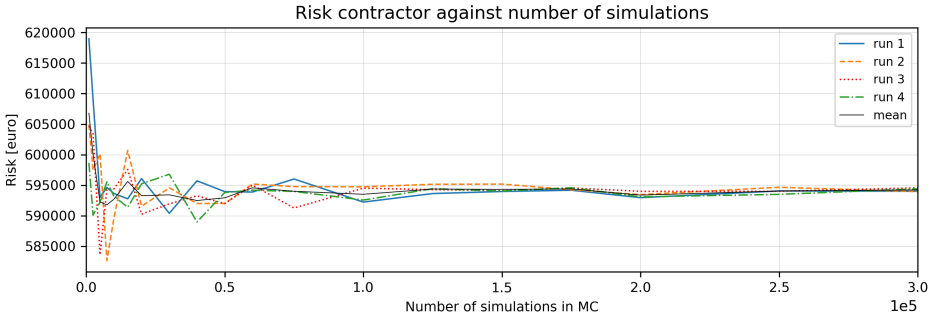

Figure 8.1: Mean risk for the contractor plotted against the number of Monte Carlo simulations.

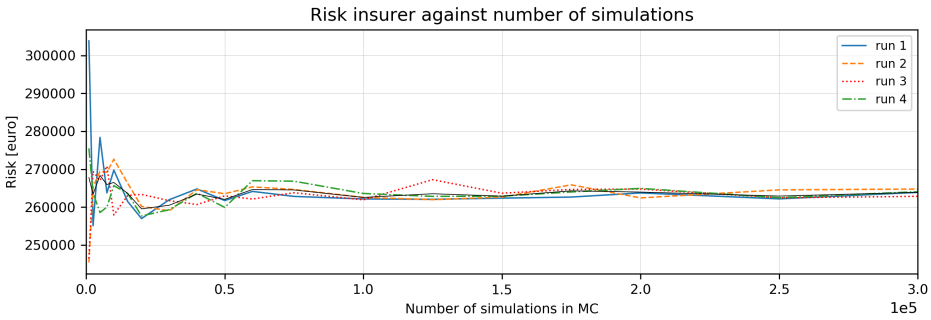

Figure 8.2: Mean risk for the contractor plotted against the number of Monte Carlo simulations.

After approximately 300,000 simulations (n) the mean value for the financial risk approaches a more or less constant value, see fig. 8.1 and 8.2. For the convenience To obtain the rest of the results in this chapter, the model uses 300,000 simulations.

8.1.3. Results base case

Though the results from the model can not be validated, they still Results are promising, they give a good feeling on what the effect is

8.2. Sensitivity starting date

8.2.1. Scenarios

As the effect of the seasonality is included in the model, the time of starting the construction works, will have an influence on the financial risk.

To investigate the sensitivity of the starting date on both the risk and project duration, twelve different scenarios are runned in the model. Each scenario starts in a different month, while the rest of the parameters is kept the same as in the reference case. All scenarios start on the third day of the concerned month.

Table 8.5: Starting dates construction work

Scenario	Start date	Scenario	Start date
1	03-01-2014	7	03-07-2014
2	03-02-2014	8	03-08-2014
3	03-03-2014	9	03-09-2014
4	03-04-2014	10	03-10-2014
5	03-05-2014	11	03-11-2014
6	03-06-2014	12	03-12-2014

8.2.2. Results

In this sections the results of the sensitivity analysis of the starting data (see section 8.2.1) are shown. The sensitivity is analysed on two different model outputs:

Figure 8.3 shows the probability of the three breakwater sections being completed in a certain number of weeks according to the start date of the construction works. The figure clearly shows a significant influence of the starting date on the required construction time. According to the results, the best month to start the construction works is in march, September turns out to be the most disadvantageous month. The difference in the probability of completion can be significant. For example; after 35 weeks, the probability of completion is nine times larger when started in the most favourable month compared to the leas favourable month.

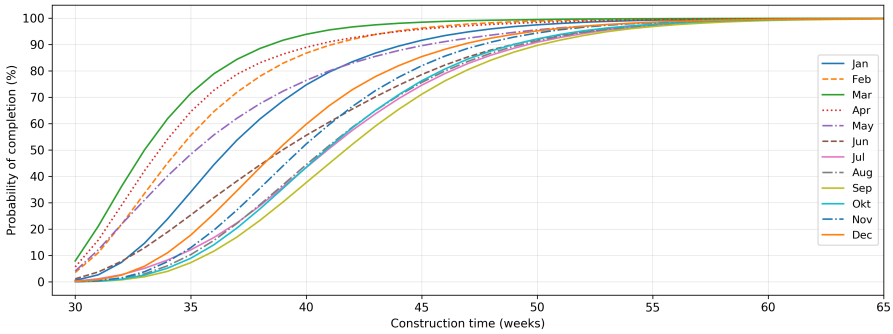

Figure 8.3: Probability of completion after a certain number of weeks. The nominal construction time is 30 weeks.

Figures 8.4a and 8.4b show the boxplots of the financial risk, according to the start date of the construction works. Figure 8.4a shows the risk for the contractor and figure 8.4b show the risk for the insurance company. In the boxplot, the mean value of the risk is shown by the green triangle, and the median is shown by the orange line. Commencing construction works in March results in the lowest financial risk for both the contractor and insurer, September results in the highest financial risk for both the contractor and insurer. This corresponds with the results from fig. 8.3.

It should be noted that the results are obtained from one older breakwater project, the reference case. Validation of the model was not possible as not all required data was available for this study; hence, no calibration could be performed. All outcomes are thus indicative and must be seen in the context of the sensitivity analysis and the feasibility of the model. The individual results, standing on their own, should not be interpreted as an absolute quantity. So, the less than 10% probability of finishing the breakwater according to the nominal construction time (see fig. 8.3), should not be interpreted as an absolute quantity.

Although both figures (8.4a and 8.4b) show the same influence by the starting date (similar shape), there are three major differences between the boxplots for the contractor and the boxplots for the insurer. First, in 8.4b some median values are equal to zero (located at y = 0). Secondly, all the boxplots (ex. September) have the first quartile (also the 25th percentile) located on the x-axis. Third, the difference between the median of the risk and the mean risk is larger for the insurance company. All three differences can be explained by the fact that in a lot of the simulations, the insurance threshold is not reached, hence a financial risk of zero Euro for the insurer.

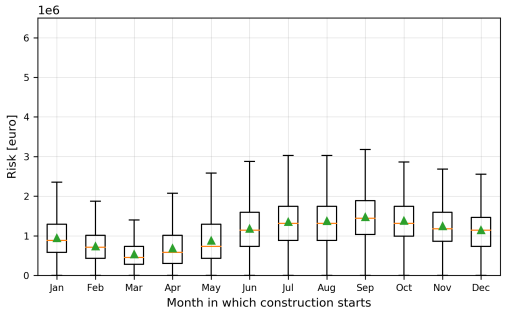

(a) Financial risk contractor

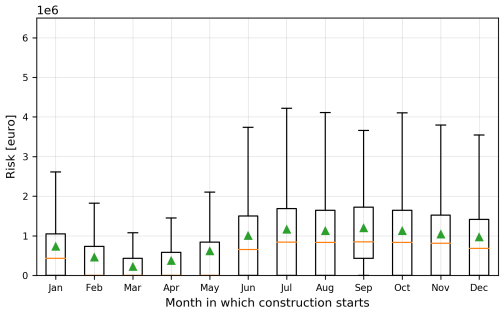

(b) Financial risk insurer

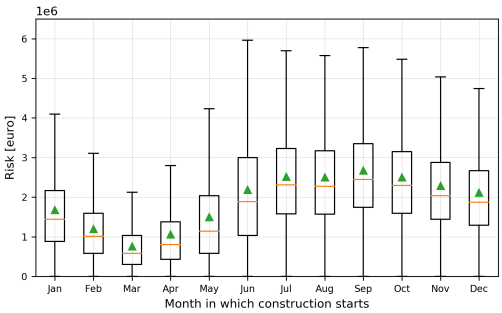

(c) Total financial risk

Figure 8.4: The boxplots of the financial risk associated with the construction phase, for every possible start month of the construction phase. This is done for the financial risk for the contractor (a), the insurance company (b), and the total financial risk (c).

Overall the result shows a strong influence of the start date on the financial risk and the project duration. The results underline the importance of including the seasonal influences in the model. In the next sections all results are obtained with a start date of 3-march 2014.

8.3. Sensitivity influenceable input parameters

8.3.1. Scenarios

The input parameters examined in the sensitivity analysis, represent a value which can be influence by changing the design or changing the work method.

By changing the mean values of the parameter distribution functions, the effect on the contractor risk and insurer risk is analysed. The following parameters are studied:

- Nominal diameter D_{n50}
- Length of the open workfront L_{of}
- repair rates R_{cap}
- Insurance threshold Ω

Nominal diameter

Three scenarios for the nominal diameter of the rock material are analysed. In the first scenario, only the sensitivity of the underlayer($D_{n50,UL}$), secondly the sensitivity of the core material ($D_{n50,c}$), and last the situation where The sensitivity on only the is changed for the underlayer, the core and

Table 8.6: Values nominal diameter per scenario

Scenario	Variable	- 20%	- 10%	Initial	+ 10%	+ 20%
1	Nominal diameter core [m]	0.2704	0.3042	0.338	0.3718	0.4056
2	Nominal diameter underlayer [m]	0.88	0.99	1.1	1.21	1.32
3	Nominal diameter core [m]	0.2704	0.3042	0.338	0.3718	0.4056
	Nominal diameter underlayer [m]	0.88	0.99	1.1	1.21	1.32

Length open front

Four scenarios for the lenght of the open fronts are analysed. Three situations where the open front of one individual section is changed, and one situation where the open fronts of all section are changed.

Table 8.7: Values open fronts

Scenario	Variable	- 20%	- 10%	Initial	+ 10%	+ 20%
1	Length open front submerged core [m]	80	90	100	110	120
2	Length open front emerged core [m]	80	90	100	110	120
3	Length open front underlayer [m]	80	90	100	110	120
4	Length open front all sections [m]	80	90	100	110	120

Repair rates

The repair rate is a parameter which can only be changed in discrete steps, as it depends on the number and type of machinery. Although Changing the repair rate with a certain percentage is not always possible, it still shows the sensitivity of the repair rate on the mean financial risk.

Since the repair rates used in the model are based on the construction rates of the reference case and adjusted by expert judgement, their values are not an absolute quantity. Hence, it becomes extra interesting to include them in the sensitivity analysis. If the repair rates turn out the have a strong influence on the financial risk, it may be desired in the future to improve the estimation of the repair rates.

Table 8.8: Values repair rates

Scenario	Variable	- 20%	- 10%	Initial	+ 10%	+ 20%
1	Landbased repair rates underlayer material [ton / week]	4800	5400	6000	6600	7200
	Marine repair rates underlayer material [ton / week]	4000	4500	5000	5500	6000
	Landbased repair rates core material [ton / week]	6400	7200	8000	8800	9600
	Marine repair rates core material [ton / week]	8000	9000	10000	11000	12000

Insurance threshold

Table 8.9: Values insurance threshold

Scenario	Variable	- 20%	- 10%	Initial	+ 10%	+ 20%
1	Insurance threshold of H_s [m]	2.8	3.15	3.5	3.85	4.2

8.3.2. Results

This sections shows the results of the sensitivity analysis described in section 8.3.2 of several input parameters on the mean risk.

Nominal diameter

Three scenarios were created to study the sensitivity of the nominal stone diameter on the mean financial risk. In scenario 1 only the D_{n50} of the core material is fluctuated (fig. 8.5a), in scenario 2 only the underlayer (fig. 8.5a), and in scenario 3 the D_{n50} for both the core and underlayer are fluctuated (fig. 8.5c).

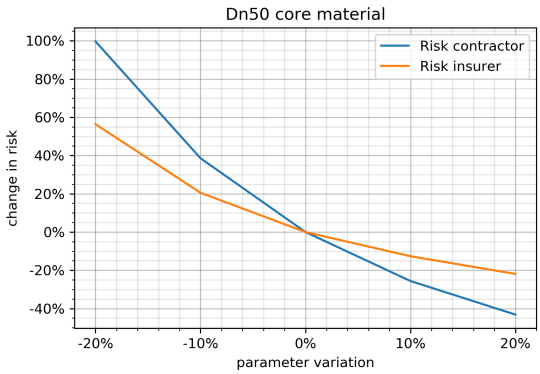

(a) Scenario 1: Sensitivity Dn50 core material

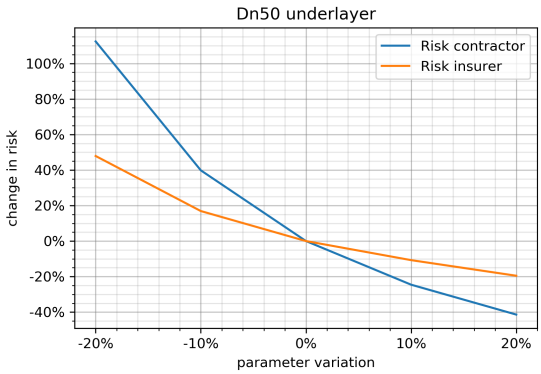

(b) Scenario 2: Sensitivity Dn50 underlayer material

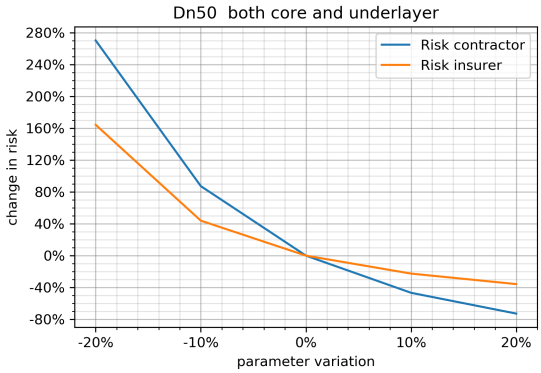

(c) Scenario 3: Sensitivity Dn50 both core and underlayer material

Figure 8.5: Three subfigures

The first thing that stands out in all three figures is the difference in sensitivity of the nominal diameter on the contractor risk and insurer risk. The sensitivity on the risk for the contractor is around as twice as large as the sensitivity on the risk for the insurance company. This difference in sensitivity could be explained by the effect changing the nominal diameter has on the probability of occurrence of a damage event.

Changing the nominal diameter has a direct effect on the probability of occurrence of a non-insurable damage event. Increasing the nominal diameter results in a larger resistance of the structure, hence larger waves are needed to initiate damage. As the climate of incident waves is not influenced by the structure, the probability of having a damage event during construction decreases. If the nominal diameter decreases, smaller waves become capable of initiating a damage event, increasing the probability of having damage events during construction. Thus changing the D_{n50} influences the financial risk for the contractor, by changing the probability of having a damage event.

This direct effect on the probability of occurrence is, however, missing for insurable damage events. For the reference case, wave conditions exceeding the insurance threshold will always result in damage to the core and underlayer section. So the probability of occurrence of an insurable damage event, only depends on the wave statistics and the insurance threshold, hence the probability of having an insurable damage event during construction remains the same. Changing the nominal diameter for the reference case, therefore has only a direct effect on the magnitude of the damage, given a certain wave condition.

The variation of the nominal diameter influences the magnitude of the damage for both the non-insurable events and the insurable damage events. However, as the variation of the nominal diameter only influences the probability of occurrence of non-insurable damage events, it has a larger sensitivity on the financial risk for the contractor than for the insurance company. Thought the insurance threshold is project-specific, it is expected that for other breakwater projects, the sensitivity of the nominal diameter on the financial risk is always more significant for the contractor than for the insurer.

Length open fronts

Four scenarios were created to study the sensitivity of the length of the open front on the mean financial risk. In scenario one the open fronts of all sections are varied (fig. 8.6a), in scenario two only the open front of the emerged core section is changed (fig. 8.6b), in scenario three only for the underlayer section fig. 8.6c and scenario four only for the submerged core section. for both the core and underlayer are fluctuated (fig. 8.6d).

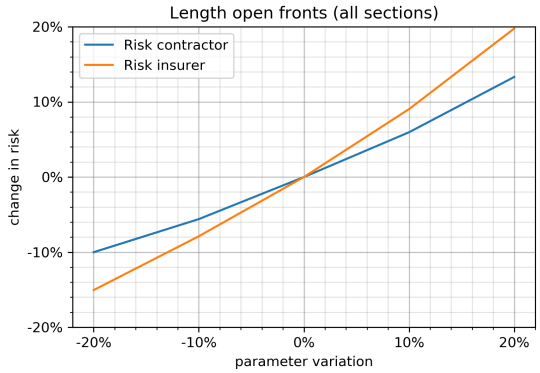

(a) Scenario 1: Variation all sections together

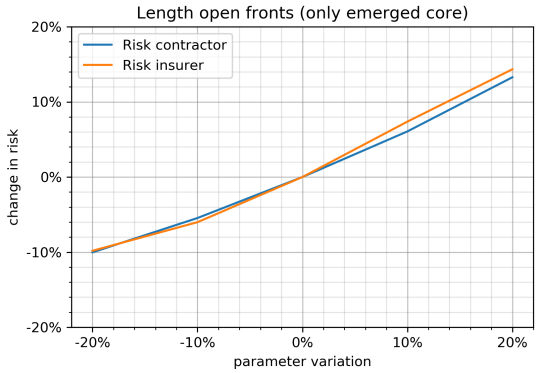

(b) Scenario 2: Variation length open front emerged core

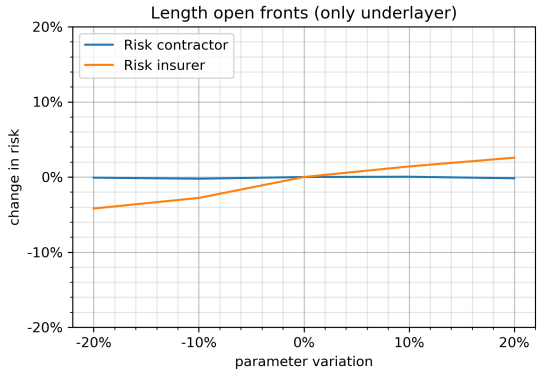

(c) Scenario 3: Variation length open front underlayer

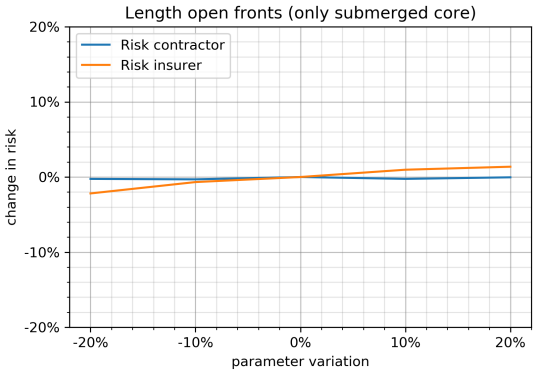

(d) Scenario 4: Variation length open front submerged core

Figure 8.6: Sensitivity of the open fronts of different the breakwater sections on the mean risk for the contractor and the mean risk for the insurance company

In fig. 8.6a, the sensitivity of the open front length of all sections together on the mean financial risk is shown. Comparing fig. 8.6b, 8.6c and 8.6d with fig. 8.6a, it can be clearly seen that most of the sensitivity in fig. 8.6a comes from the emerged core. This can be explained by the fact that all damage events start with damage to the emerged core section, not all damage events contain damage to the other two sections. So the number of damage events to the submerged core and underlayer is significantly smaller compared to the emerged core section.

The sensitivities of the open front of the underlayer and submerged core, on the mean financial risk for the contractor, displayed in fig. 8.6c and 8.6d are quite surprising. Apparently, the sensitivity on the mean financial risk for the contractor is almost zero, while this is not the case for the insurer risk. No explanation on this difference is found. It is therefore recommended to further investigate this result in future studies, such in order to confirm the result are correct or to find missing damage mechanisms.

Repair rates

To study the sensitivity of the repair rates on the mean financial risk, one scenario was introduced. In this scenario both the marine and landbased repair capacities for the core and underlayer where varied. The result is shown in fig. 8.7.

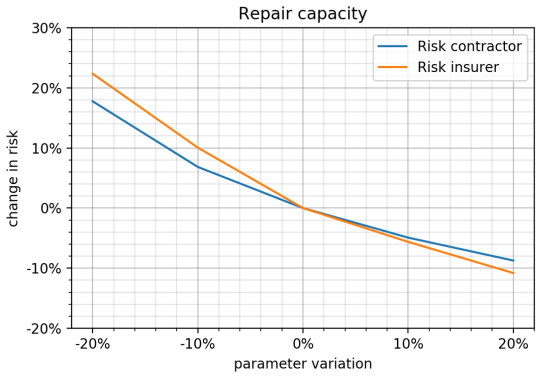

Figure 8.7: Sensitivity of the repair rates (ton/week) on the mean financial risk for the contractor and the mean financial risk for the insurance company.

According to the result in fig. 8.7, the sensitivity of the repair capacities on the mean financial risk is larger for the insurance company, than for the contractor. Although repair rates can only be changed in discrete steps, the result of the sensitivity is quite interesting. Since the repair rates are based on the construction rates and expert judgement, they contain some uncertainty. For the reference case, an uncertainty of 10% in the repair rates, result in an uncertainty up to 7% for the mean financial risk for the contractor and up to 10 % for the mean financial risk for the insurance company. Tough the result is case-specific, it can be concluded in general that the repair capacity contributes to the uncertainty in financial risk for both the contractor and the insurer. Estimating the repair rates in the model for future projects should be done with extra caution

Insurance threshold
The result of the sensitivity analysis for the insurance threshold Ω is shown in fig. 8.8.

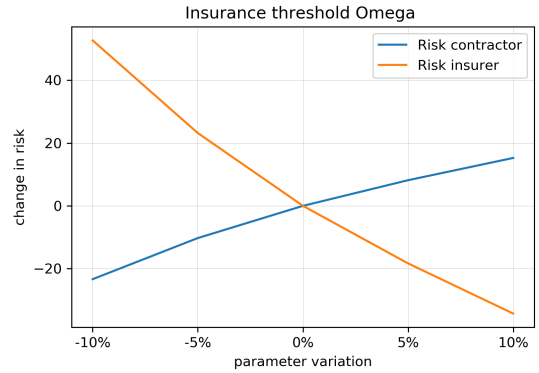

Figure 8.8: Sensitivity of the insurance threshold of the mean financial risk for the contractor and the insurance company.

As the mean financial risk for contractor is not the same as the mean financial risk for the insurance company, the percentage change is not equal to each other.

8.4. Fomula parameter sensitivity

8.4.1. Scenarios

The reliability functions introduced in chapter 5, all contain a non-dimensional damage parameter. These parameters represent the minimum level of reshaping, which is considered as a damage event. For the submerged core and the underlayer, this parameters is the damage value S_d, and for the emerged core, this is the damage threshold parameter D_t. The minimum level of reshaping, representing the start of damage, is not fixed. A contractor may accept some larger amount of reshaping as the start of a damage event if machinery on location makes it possible to repair this damage during the construction work itself.

Table 8.10: Values for the damage parameters

Scenario	Variable	-2	-1	Initial	+1	+2	+3
1	Damage parameter underlayer & submerged core	-	1.0	2.0	3.0	4.0	5.0
2	Damage threshold emerged core	3.0	4.0	5.0	6.0	7.0	-

8.4.2. Results

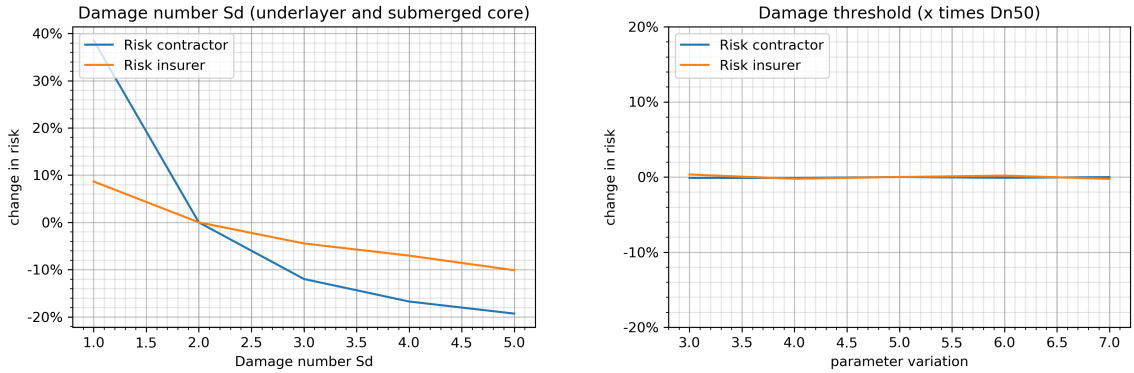

(a) Risk contractor

(b) Risk insurer

Figure 8.9: Histograms of the weekly maximum wave height for each season.

The result from fig. 8.9a is in line with expectations. The larger the amount of reshaping is allowed to be considered as no damage, the smaller the financial risk becomes, and vice-versa. The results from fig. 8.9b are not that straight forward. Apparently there On possible explanation is that as soon the reshaping of the emerged core start, horizontal shift of the local origin (introduced in section 5.3.3) is almost always larger than the set three to seven times the nominal diameters (D_{n50}). It is recommended to further investigate this result in future studies, such in order to confirm the result are correct or to find other explanations for the result.

9

Discussion

The objective of this research is to investigate the feasibility of a model with which risks related to the construction phase of rubble mound breakwaters in sea-state conditions can be determined. This chapter provides a discussion about the relevance of this research, its results, and considerations made in this study.

9.1. Geotechnical failure

During the construction, geotechnical failure is the second important mechanism for damage after storm events (Maddrell, 2005). In this study, the focus has been on damage due to storm events, other possible mechanisms that could lead to damage have not been taken into account. However, in some situations, geotechnical failure can be triggered by pressure differences due to waves during a storm event (Maddrell, 2005). It is challenging to make a distinction between when the failure is due to the storm event or due to shortcomings, like a faulty design or insufficient soil improvement methods. In a follow-up to this study, the model could be expanded with this, if desired.

9.2. storm surge

In the model, the storm surge is not included. For the reference case, this decision is considered valid, though it could be seen as a slightly conservative approach.

When the model is used for other projects, the storm surge can become important, as it is very location-specific. Especially for situations located in shallow water, storm surge can result in larger wave heights. Neglecting the storm surge in these situations would result in a severe underestimation of the storm-induced damage.

For validating the result of the proposed method for the emerged core (see fig. 5.8), a storm surge was added to the mean water level. According to the design wave conditions report (internal documents Van Oord, 2013), the storm surge should be 0.6 meters for the direction the waves were coming from.

9.3. Insurance coverage

In order to claim the insurance, the damage must have been caused by a storm event whose wave conditions have exceeded the insurance threshold. It is the contractor's responsibility to prove that the wave conditions during the storm have exceeded the insurance threshold.

Practice shows that even in the situation the contractor can prove the exceedance of the insurance threshold, a discussion can arise about the cause of the damage, and the party responsible for it (personal communication Van Oord, 2019). Especially in situations where the contractor was only responsible for the construction, disputes can arise between the designing party, the contractor and the insurer. Due to their sensitivity, details on these disputes will not be discussed further. If the parties are not able to agree on the situation, the conflict can be resolved via arbitration. It is therefore extremely important for employer, contractor and insurer to agree to the specific conditions and definitions of the insurance policy before construction starts.

What can be mentioned is that in practice, it rarely happens that the insured party receives 100% coverage for the claimed damage (Tanis, 2019). The model (introduced in chapter 3) does not take this into account since it was outside the scope of the study. As a result, the actual risk may be higher than the risk calculated by the model. On top of that, any legal costs incurred will lead to a higher risk.

In a follow-up study, this could be included taking a certain percentage of the insured risk and add it to the uninsured risk. This percentage should be based on expert judgement, and probably include a stochastic behaviour, to represent its uncertainty.

9.4. Model setup

9.4.1. Subsequent damage event during repair period

A damage event may occur during the repair period of a previous damage event. In such situations, the damage strongly depends on the state of progress of the repair works, since the cross-sectional shape of the breakwater has a strong influence on the resistance of the structure.

In the model, however, during the repair period, the actual cross-sectional shapes of the breakwater sections are unknown. The model only knows at which time-step the repair works are completed, but does not simulate the actual repair progress. To overcome this problem and make it possible for the model to determine the amount of damage, a more conservative approximation is applied.

If in the model, a subsequent damage event happens at a time-step repair works are continuing; the model calculates the amount of damage as if the breakwater was intact before this second event. This may overestimate the amount of damage.

9.4.2. Seasonality

As described in section 3.2, the return period of a particular hydraulic event is non-stationary over the year. To include the non-stationary behaviour of the wave climate in the model, the distribution functions for the wave height and period were obtained for each meteorological season, instead of the entire year.

Results from the sensitivity analysis show a clear and strong influence of the seasons on the project duration, mean financial risk and frequencies of damage events during construction. Despite the fact that validation was not possible, the model does show credible results.

Instead of obtaining the distribution functions for the wave height and wave period for the four meteorological seasons, they could also be obtained for all 12 months. This Increases the accuracy of the non-stationary behaviour of the wave climate in the model. A downside of dividing the weekly maximum data over 12 months is that it will decrease the accuracy of the fitted theoretical distribution functions as the number of data points to fit these distribution function decrease.

Hence, there is Trade-off between the accuracy of the non-stationary behaviour and the accuracy of the obtained distribution functions.

9.4.3. Variable construction rates

For the contractor, there is a constant trade-off between building efficiency and potential damage due to storms. The larger the open work front, the more efficient the building method, as the deployment of machinery is less likely to be delayed by slow progress in other sections and therefore shortening the time needed for construction. Comparatively short work fronts, on the other hand, lead to machinery working closer together and a less efficient building method. However, the longer the open work fronts, the larger becomes the financial risk, increasing damage after a storm drastically. So the trade-off boils down to balancing building efficiency against the risk attended with exposure to storms.

In the model, the open work fronts of the breakwater sections all have the same construction rate, resulting in that no such trade-off is included. Adding variable construction rates to the work fronts, and the costs of waiting for previous work fronts enables the model to find an optimum length for the open work fronts.

9.5. Schematization factor

There is, of course, a difference between the physical tests used to compose the damage formulas and the actual situation. To deal with any discrepancies, a schematization factor can be added. For this study, the

model had a schematization factor of 1, as this schematisation factor was outside the scope of the research. If the model is used in the future for other breakwater projects, this schematization factor can be changed to deal with any discrepancies.

9.6. Sensitivity analysis

The report does not claim completeness in the sensitivity analysis, as not all parameters have been tested. However, for the purpose of this research, namely the feasibility of a model to determine the financial risk, the sensitivity analysis is considered adequate.

10

Conclusion and recommendations

In this chapter the conclusions and recommendations of this study are described. Section 10.1 contains the conclusions, followed by the recommendations in section 10.2.

10.1. Conclusion

The aim of this study is to investigate the feasibility of a model with which uninsured risks related to the construction phase of rubble mound breakwaters in sea-state conditions can be assessed. To draw a conclusion towards the research objective, the research questions are answered in the following sections.

Damage mechanisms

The first question that needs to be answered is, what are the damage mechanisms related to the construction phase of a rubble mound breakwater, during storm conditions. To answer the question it has to be realized that behind the open fronts, the breakwater should in principle be able to withstand the design conditions. These design conditions are far more substantial than the insurance threshold as insurance loses its purpose if the threshold conditions are larger than for which the structure is designed. If damage occurs it will consequently always be covered by the CAR insurance. In terms of risk for the contractor, therefore, only the open front sections of the core and underlayer are relevant, and the answer is therefore focused on these sections. For the reference case, the following damage mechanisms have been distinguished:

- Reshaping of the submerged core due to head on and oblique wave attack
- Reshaping of the emerged core due to head on and oblique wave attack
- Rashaping of the underlayer due to head on and oblique wave attack.
- Mixing of rock material of different sections.
- Overwash of dislocated material.

From literature study provided in chapter 5, reshaping of the emerged and submerged core can only be calculated for situations with head on wave attack.

Quantitative damage calculations

Quantitative damage calculations are needed to compute the magnitude of damage to the different open work fronts. For each section the conclusion is given.

Underlayer section

To calculate the magnitude of damage to the underlayer section, the stability formulas of Van der Meer (1988) for rubble mound armour layer can be used. The underlayer is modelled as a small armour layer. By inverting these formulas, the area of erosion can be written as a function of storm conditions.

Emerged core section

Damage to the open emerged core section can be calculated by modelling this section as a dynamically stable reshaping rubble mound slope. Both Van der Meer (1988) and Merli (2009), provided .„„ where Merli adjusted the relations, found by Van der Meer for rock material with very wide grading. Mulders (2010) proved that for large gradings, like quarry run, Van der Meer (1988) tends to underestimate the amount of reshaping and that Merli is more suitable.

In the current available literature no information has been found that covers the following two situations:

1. The amount of reshaping of the core material in the underlayer section, when the underlayer is breached.
2. Recession of the crest, larger than the initial crest width.

From a survey of past projects (personal communication Van Oord, 2019), these two damage situations are quite prominent and cannot be neglected. Two newly developed methods to calculate the damage in both situations turned out to quite promising.

The amount of reshaping of the core after breaching of the underlayer can be calculated by first determining the amount of waves needed to breach the underlayer. Next this amount of waves needed to breach the underlayer is subtracted from the total number of waves characterizing the storm event. The remaining number of waves is then used to compute the reshaping of the exposed core. Result form this method shows a reshaping profile, which is very close to the post storm situation of the reference case (see section 5.3.4).

In the situation the crest recession is larger than the initial crest width, the mass balance no longer applies. By assuming the crest to be infinitely long, the reshaping of the crest can by computed as the mass balance still holds. Results from this method shows almost the same reshaping profile as the physical experiments form Merli (2009).

Submerged core section

The method of Wallast and van Gent (2002) was superior to the many other methods to describe the amount of reshaping of the submerged core section. Modelling the submerged core section as a near-bed structure by Wallast and van Gent (2002), the validity range sometimes becomes an issue depending on the storm conditions. With the introduced adjustment in section 5.4.4 to solve this issue, it has been made applicable for the simulation model. For future rubble mound breakwater projects, it is expected the same methods can be applied for quantitative damage calculations to the submerged core section.

Positive feedback in fully probabilistic model

In the currently available literature no method was found to calculate the risk, which includes the positive feedback between the delay and the probability of a subsequent damage event. In this study, therefore, a method is created, where a fixed time-step stochastic model simulates the construction phase. Simulating the construction process enables it to include the positive feedback between delay due to damage, and the increase in the probability of encountering unfavourable conditions in the remaining construction time. Due to the stochastic behaviour of the parameters used in the building process simulation, the simulation outcome itself is characterised by a stochastic behaviour. It is therfore combined with a Monte Carlo simulation.

Due to the stochastic behaviour of both the strength of the structure and the hydraulic conditions, it is not possible to define a damage event on beforehand, hence using a discreet event simulation becomes really difficult, if not impossible. The fixed time step simulation is therefore considered the best method to simulate the construction progress.

Sensitivity

Before answering the question which damage mechanisms and breakwater parameters correspond with the largest risk, it needs to be stated that according to the results from the sensitivity analysis, there is a difference in sensitivity on the financial risk for the contractor and the financial risk for the insurance company. As the topic the study is on the financial risk for the contractor, the conclusion is focussed on the sensitivity for the contractor. Conclusions are given for the reference case, and the general situation.

The input parameters with the strongest sensitivity on the financial risk are the nominal diameter for core and underlayer material, and the start date of construction works. For the reference case, the difference in mean financial risk between the most favourable and least favourable starting month is more than 140%. Furthermore, the difference in the probability of completion was significant. For example; after 35 weeks, the probability of completion was nine times larger when started in the most favourable month compared to the least favourable month.

Though the magnitude of the sensitivity is case-specific, there is a strong indication that this effect holds for other breakwater projects in climates with a clear difference between seasons as well. So, in general, it can be concluded that the start date of construction work has a strong influence on the financial risk end project delay for breakwaters located in areas with clear seasons. The results underline the importance of including the seasonal influences in the model and risk calculations used for future breakwater projects.

According to de model results, the breakwater parameter with the largest sensitivity on the financial risk for the reference case was the nominal diameter. Increasing the nominal diameters with only 2% resulted in a decrease of the mean financial risk for the contractor by 10%, an effect with a factor five. While the magnitude of sensitivity is case-specific, there is a strong indication, that of all the breakwater parameters, the nominal diameter has the largest sensitivity on the financial risk in general.

Furthermore, the sensitivity of the nominal diameter on the mean financial risk for the contractor was around twice as large than for the insurance company. This difference in sensitivity can be explained by the effect changing the nominal diameter has on the probability of occurrence of a damage event. Changing the nominal diameter has a direct effect on the probability of occurrence of a non-insurable damage event, where due to the insurance threshold this direct effect on the probability of occurrence of a insurable damage event was neglectable. Thought the insurance threshold is project-specific, and magnitude in sensitivity can differ, it is expected that for other breakwater projects, the sensitivity of the nominal diameter on the financial risk is always stronger for the contractor than for the insurer.

Reshaping of the emerged core corresponds with the largest financial risk. Following from the models result, the most sensitive breakwater component during construction is the open emerged core section. For every damage event, damage started at the emerged core section.

10.2. Recommendations

The recommendations are split in two different categories, namely the recommendations for further research into this topic section 10.2.1 and the more ‘practical’ advices for contractors, described in section 10.2.2

10.2.1. Further research

Construction speed and costs
It would be interesting to expand the research by making the construction speeds for the different open sections independent and adding construction costs to the model.

In this way, it is possible to investigate more options for the construction method. The ultimate goal of this study direction is to create an optimization between the construction methods and the financial risk due to damage events. This thesis can then be seen as the first phase for this ultimate goal.

Validation of proposed method
The proposed method for the situation were literature was not sufficient enough, turned out to be quite promising. It will be interesting to validate the two proposed methods for the emerged core. Physical test would be required to test the situation.

More case projects
For the reference case the model shows good results. In order to obtain more general conclusions, more breakwater projects are needed. As the amount of project, confronted with damage during the construction phase among one contractor is limited, contractors could work together in order to obtain data of more breakwater projects.

Variable construction rates
In the real situation there is a trade-off between the building efficiency against the financial risk attended

with exposure to storms. In the model, the open work fronts of the breakwater sections all have the same construction rate, resulting in that no such trade-off is included. Adding variable construction rates to the work fronts, and the costs of waiting for previous work fronts enables the model to find an optimum length for the open work fronts.

Oblique waves
The introduced damage calculations shows good and promissing results. Still they could be improved by including damage due to oblique wave attack. As soon oblique waves are included into the model, not only reshaping of the structures , also the longshore transport becomes important. It is recommended that in a follow-up of this study, longshore transport is included, and that for the damage mechanisms of

If model tests are performed in the future, they should start with the emerged core section. As the emerged core is the most sensitive open front of the breakwater, contribution the most to the financial risk.

10.2.2. Practical aspects

Nominal diameter
The sensitivity analysis (chapter 8) shows the strong sensitivity of the nominal diameter of the core material on the financial risk for the contractor. The damage mechanisms of submerged core have the smallest influence on the financial risk for the contractor, hence However for the emerged core section it is Increasing the nominal diameter of the rock material It is therefore recommended to look for an optimization between a increase in the nominal diameter, reducing the financial risk and the increasing costs for the rock procurement.

Overwash
During the storm of the reference case, mixed material (underlayer en core material) was deposited on the rear slope due to overwash. Unfortunately, part of the rear slope armour units had already been installed. The contamination of the rear armour, complicates and extends the required repair works. To prevent such situations from happening in the future, it is advised to start with the rear slope armour layer only when the front slope is already protected.

Precautionary measures
The mixing of different rock material due to breaching of the underlayer created an extra cost due to the required procurement of new rock material, and the higher costs for handling larger rocks. Usually, a storm can be predicted up to some days in advance. Depending on the expected wave conditions, the contractor could anticipate to weather forecast to minimize the potential risk. Van Oord is already doing this, however for marine contractors in general the following is still advised.

If wave conditions are expected that most likely result in only damage to the emerged core section, the contractor should try to cover as much as possible of the emerged core with the underlayer. If wave conditions are expected that are more severe and probably will result in the breaching of the underlayer, the contractor could try to remove as much as possible of the underlayer material from the underlayer section, as no or less mixing of material will occur. This is already done by contractors, however

Bibliography

Ahrens, J. P. (1987). Characteristics of reef breakwaters. Technical report cerc-87-17, US Army Corps of Engineers, Coastal Engineering Research Center, Vicksburg, Mississippi.

Balas, C. E. and Ergin, A. (2002). Reliability-based risk assessment in coastal projects: Case study in turkey. *Journal of Waterway, Port, Coastal, and Ocean Engineering*, 128(2):52–61.

Carter, D. J. T. and Challenor, P. G. (1981). Estimating return values of environmental parameters. *Quarterly Journal of the Royal Meteorological Society*, 107(451):259–266.

CIRIA; CUR; CETMEF (2007). *The Rock Manual. The use of rock in hydraulic engineering*. C683, CIRIA, London, 2nd edition edition.

de Pater, P. (2019). personal communication, Van Oord.

Gent, M. R. A. V., Smale, A. J., and Kuiper, C. (2004). *Stability of Rock Slopes with Shallow Foreshores*, pages 100–112.

Kao, J. and Hall, K. (1990). Trends in stability of dynamically stable breakwaters. In ASCE, editor, *22nd International Conference on Coastal Engineering*, pages 1730 – 1741, Delft, The Netherlands.

Law, A. M. and Kelton, W. D. (2015). *Simulation Modeling and Analysis*. McGraw-Hill Higher Education, 5th edition.

Lomónaco, P. (1994). Design of rock cover for underwater pipelines. Master thesis, International Institute for Infrastructural Hydraulic and Environmental Engineering (IHE), Delft, The Netherlands.

Maddrell, R. J. (2005). Lessons Re-Learnt from the Failure of Marine Structures. *International Conference on Coastlines, Structures and Breakwaters 2005*, pages 1–15.

Menéndez, M., Méndez, F. J., Izaguirre, C., Luceño, A., and Losada, I. J. (2009). The influence of seasonality on estimating return values of significant wave height. *Coastal Engineering*, 56(3):211 – 219.

Merli, D. (2009). Stability of wide-graded rubble mounds. Master thesis, UNESCO-IHE, Delft, Netherlands.

Mulders, P. (2010). Breakwaters under construction exposed to oblique waves. Master's thesis, Delft University of Technology, Delft, Netherlands.

PIANC(2003). State-of-the-art of designing and constructing berm breakwaters. Report of wg 40, 2003, MarCom, International Navigation Association, Brussels, Belgium.

Powell, K. A. and Allsop, N. W. H. (1985). Low-crested breakwaters, hydraulic performance and stability. Report SR 57, Hydraulic Research Wallingford, Oxfordshire OX10 8BA.

Saltelli, A. (2008). *Global sensitivity analysis: the primer*. John Wiley.

Smith, G. M. (2018). personal communication, Van Oord.

Tanis, D. (2019). personal communication, Van Oord.

Tørum, A., Kuhnen, F., and Menze, A. (1990). On berm breakwaters. stability, scour, overtopping. Report no h986, q638, wl, Delft Hydraulics, Delft.

van der Meer, J. (1990). Low-crested and reef breakwaters. Report no h986, q638, wl, Delft Hydraulics, Delft.

Van der Meer, J. W. (1988). *Rock slopes and gravel beaches under wave attack*. PhD thesis, Delft University of Technology.

van der Meer, J. W. (1998). Applications and stability criteria for rock and artificial units. In Pilarczyk, K., editor, *Seawalls, dikes and revetments*, chapter 11. A.A. Balkerma Publisher, Rotterdam.

Van der Plas, T. and van der Meer, J. (2017). Stability of very wide graded material, designed as breakwater core, under wave attack.

Van Oord (2013). Unpublished internal document.

Van Oord (2014). Unpublished internal document.

Van Oord (2019). Photo archive Celum.

Vidal, C., Losada, M. A., and Mansard, E. P. D. (1995). Stability of low-crested rubble-mound breakwater heads. *Journal of Waterway, Port, Coastal, and Ocean Engineering*, 121(2):114–122.

Vidal, C., Medina, R., and Martin, F. (2000). A methodology to assess the armour unit stability of low-crested and submerged rubble-mound breakwaters. In Losada, I. J., editor, *Coastal Structures '99*, volume 2. Balkema.

Wallast, I. and van Gent, M. (2001). Stability of near-bed structures and bed protections; analysis of physical model tests with waves and currents. Delft cluster report dc030204/h3804, Delft Hydraulics, Delft, The Netherlands.

Wallast, I. and van Gent, M. R. A. (2002). Stability of near-bed structures under waves and currents.

List of Figures

List of Tables

A

Stochastic variables

This appendix gives an overview of all stochastic parameters.

Table A.1: General input variables

Variable	Symbol	Distribution
Hydraulic variables		
Significant wave height [m]	ρ_w	GEV
Mean wave period [s]	ρ_w	Normal
Other variables		
Number of waves [-]	N	Normal
Slope [°]	α	Normal
Nominal diameter underlayer [m]	$D_{n50,ul}$	Normal
Nominal diameter core [m]	$D_{n50,c}$	Normal
Density of stone [kg/m^3]	ρ_s	Normal
Density of water [kg/m^3]	ρ_w	Normal
Plunging coefficient, deep water [-]	$c_{pl,d}$	Normal
Surging coefficient, deep water [-]	$c_{s,d}$	Normal
Plunging coefficient, shallow water [-]	$c_{pl,s}$	Normal
Surging coefficient, shallow water [-]	$c_{s,s}$	Normal

B

Insurance

This appendix give a brief introduction about the **Construction All Risks (CAR) insurance**.

The care of the Works is in principle the risk and responsibility of the Contractor. This risk can be covered by a CAR insurance (Insurance for the Works) In order to arrange a CAR insurance detailed project information is required, such as but not limited to:

- Scope of work
- Working method
- Estimated Contract Value & Quantities
- Design
- Construction period & Defects Notification Period
- Parties involved

It is a duty of the insured to provide all material information because based on this information insurers determine the risk profile of a project

This information will be shared with an insurance broker and subsequently the insurance broker shall try to find insurance companies who are willing to accept the risk at the best possible terms and conditions. The risk is normally shared amongst a panel of insurers, whereby the leading underwriter is setting the terms and conditions (ie premium, deductible, special conditions, etc)

A CAR insurance consists of a Cover Note and Insuring Conditions. On the Cover Note (Policy Schedule) the project specific details and special terms and conditions are mentioned. The Insuring Conditions are the general terms and conditions.

In case of a material change of the project information (such as but not limited to change in scope / working method / planning) insurers have to be notified, otherwise a claim can be rejected or the policy can even be withdrawn.

A CAR insurance normally contains the following coverages:

- Section I: physical loss/damage to the Works - insured limit full contract value
- Section II: TPL arising out of the execution of the Works – insured limit e.g. EUR 5,000,000
- Section III: loss/damage to Employer's existing property – insured limit e.g. EUR 5,000,000

The level of deductibles in case of loss or damage to the Works (Section I) depend on the type of Work and risks, but are generally as follows:

- Major Perils/Acts of God: min EUR 250,000 each occurrence - All other losses: min EUR 100,000 each occurrence

The premium is always a certain percentage of the contract value, but also very much depending on the type of Work, risks involved, contract value, etc. On a general note we could say the following:

- 0.20% - 0.30% for a dredging and reclamation project - 0.50% - 0.75% for rock works (breakwater, revetment, etc)

C

Literature

This appendix provides extra insight in the literature study on the emerged core section and the submerged core section

C.1. Emerged core section

In this section an explanation is provided why the method of Ahrens (1987) is not suitable for the damage calculations to the submerged core section.

Crest recession

Kao and Hall studied the reshaping of dynamically stable breakwaters in respect to the variation in armour stone (changing grading and shape), wave characteristics and duration of attack. Experiments were done in a two dimensional wave flume, focus on head on waves. With a multi-variate regression analysis on their measured data, Kao and Hall (1990) set up formulas for the estimation of the estimation of the toe accretion and the recession of the berm. For the latter the formula is as follow:

$$\frac{Rec}{D_{50}} = -12.4 + 0.39\left(\frac{H_s}{\Delta D_{50}}\right)^{2.5} + 8.95\frac{D_{85}}{D_{15}} - 1.27\left(\frac{D_{85}}{D_{15}}\right)^{2} + 7.3P_R \tag{C.1}$$

Equation C.1 is based on 3000 waves, so to include the effect of different numbers of waves, a correction factor can be used to define the recession relative to the number of waves:

$$\frac{Rec_N}{Rec_{3000}} = 1 + 0.111\ln\frac{N}{3000} \tag{C.2}$$

As eq. (C.1) consists a quadratic expression, the relation between the grading and recession is represented by a parabolic function. By keeping the other parameters constant, the relation between the grading and recession is shown in fig. C.1, where the green area shows the validity range of the grading by the performed tests. A maximum berm recession is seen for gradings around 3.5.

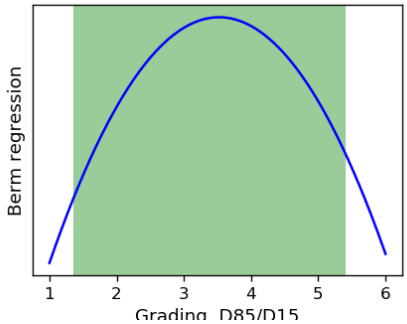

Figure C.1: Trend of the berm recession as a function of grading according to Kao and Hall.

Torum

$$\frac{Rec}{D_{n50}} = 0.0000027\left(H_0 T_0\right)^3 + 0.000009\left(H_0 T_0\right)^2 + 0.11\left(H_0 T_0\right) - f\left(\frac{D_{85}}{D_{15}}\right) - f\left(\frac{d}{D_{n50}}\right) \tag{C.3}$$

where:

$$f\left(\frac{D_{85}}{D_{15}}\right) = -9.91\left(\frac{D_{85}}{D_{15}}\right)^2 + 23.9\frac{D_{85}}{D_{15}} - 10.5 \tag{C.4}$$

$$f\left(\frac{d}{D_{n50}}\right) = -0.16\left(\frac{d}{D_{n50}}\right) + 4.0 \tag{C.5}$$

Equation C.4 consists a quadratic expression, hence the relation between the grading and the recession is represented by a parabolic function. In fig. C.2 this relation is shown, where the green are shows the validity range of the grading by the performed tests. The difference with the formula of Kao and Hall (1990), is that this parabola is a downward opening parabola, with a maximum berm recession around a grading of 1.2.

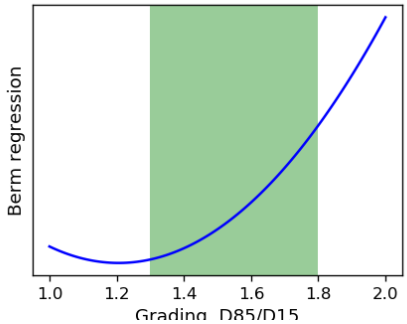

Figure C.2: Trend of the berm recession as a function of grading according to Tørum et al.

A simple but rough method to use the berm recession to compute the erosion area is to calculate the area between the point of recession and the point where the reshaped profile intersects with the initial slope (see fig. C.3). The point of intersection variates given the wave conditions and structural parameters, and no method to calculate this point was provided by Kao and Hall (1990). Tørum et al. (1990), did provide a relationship between the depth of this point and the structural parameters (h_f in fig. C.3). Merli (2009) , founded however that when extrapolating eq. (C.3) for larger values of the grading, the formula produces unrealistic high values for the recession, which was around 10 times the observed values from the physical tests. Thus non of the berm recession given formulas can be used to provide an estimation of the erosion

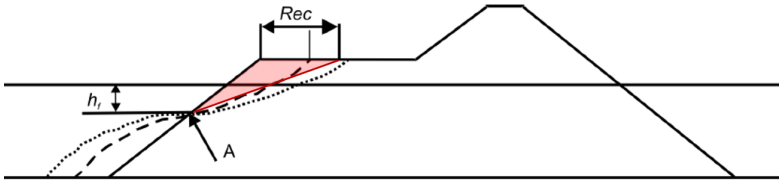

Figure C.3: Recession on a reshaping berm (PIANC, 2003), the red area indicates the simplified erosion area. Edited by author

Following from the results of Tørum et al. (1990) the effect of grading on the reshaping is clearly noticeable. The effect of grading should therefore not be neglected. Although it follows form Tørum et al. (1990) that the smallest crest regression corresponds with a grading of 1.2, and from Hall the largest recession corresponds with a grading of

conclusion So to conclude, the current available knowledge about berm/crest recessions is not usable to construct a reliable prediction for the eroded area due to wave attack. The formulas and experiments do however shows the significant influence of the grading on the crest recession, and therefor the importance of carfullness. It should therefore not just be simply used for calculated reshaping of wide graded material.

C.2. Submerged core section

Dynamically stable low crested structure (Ahrens and van der Meer)

Dynamically stable reef type structures are submerged breakwaters where some reshaping due to wave attack is allowed. They usually are consisting of homogeneous piles of armour stones, and do not have a core and underlayer. In the sense of not having different layers (missing core and underlayer), the submerged core of the rubble mound breakwater can be compared with the dynamically stable reef breakwater. However, where the dynamically stable reef breakwater is built with armour stones with a small difference in gradation, is the core of the breakwater build with quarry run with a large gradation.

Ahrens (1987) and van der Meer (1990) analysed the stability of these structures, concentrated on the change in crest height due to wave attack. Based on physical model tests, Ahrens (1987) defined a non-dimensional parameter d/d_0 to describe the behaviour of the structure, with d as the crest height after the test, and d_0 as the height before the test. It describes the change in crest height.

The crest height d can be described with the equation below:

$$N_s^* = N_s\left(H_s/L_s\right)^{-1/3} = \frac{H_s}{\Delta D_{n50}}\left(H_s/L_s\right)^{-1/3} \tag{C.6}$$

$$d = \sqrt{A_t \exp(-aN_s^*)} \tag{C.7}$$

$$a = -0.028 + 0.045C_0 + 0.034\frac{d_0}{h} - 6\cdot 10^{-9}N_b^2 \tag{C.8}$$

$$\underbrace{-0.028 + 0.045C_0 + 0.034\frac{d_0}{h}}_{\text{Magnitute of } 10^{-1}}$$

Where:

C_0	=	as-built response slope, $C_0 = A_t/d_0^2$	[-]
d_0	=	as-built crest height	[m]
h	=	water depth at the structure toe	[m]
N_b	=	bulk number, $N_b = A_t/(D_{n50})^2$	[-]

If eq. (C.7) gives a larger value of d than d_0, then d should become equal to d_0.

Table C.1: Range of validity of eq. (C.7) and eq. (C.8). The values in red indicates where the parameters of the reference project are outside the validity range.

Parameter	**Symbol**	**Range**
Response slope	C_0	1.5 – 3
Bulk number	N_b	200 – 3500
Non-dimensional freeboard	R_c/D_{n50}	-2.9 – 3.6
Non-dimensional freeboard	R_c/H_s	-1.0 – 5.5
Non-dimensional crest width	B/D_{n50}	3 – 9
Non-dimensional structure height	d_0/h	0.8 – 1.4

When applying the formulas on the reference project, the calculated relative crest height goes to infinity. It is found that this is due to the bulk number N_b. The combination of the large dimension of the cross-section and the relatively small rock material results in a bulk number far outside its validity range. For large values of N_b, the empirical parameter a becomes a negative number. Due to the minus sign before a in eq. (C.7), a becomes positive, hence the exponent goes to infinity. The relation between relative crest height d/h and the bulk number N_b is shown in fig. C.4, where the blow-up can be seen.

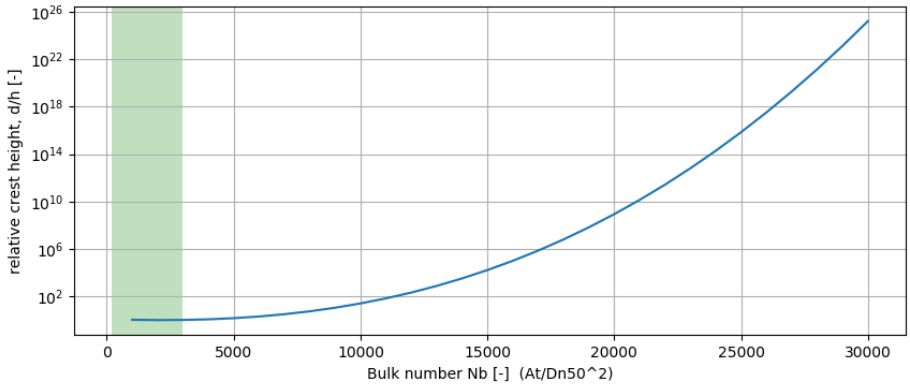

Figure C.4: Relation between the bulk number N_b and the relative crest height d/h. The green area shows the validity range for the bulk number.

D

Damage calculations

D.1. Emerged Core

For the calculations to the emerged core section, the method to satisfy the mass balance differs depending on the reshape situation.

D.1.1. Different reshaping situations

Depth limited

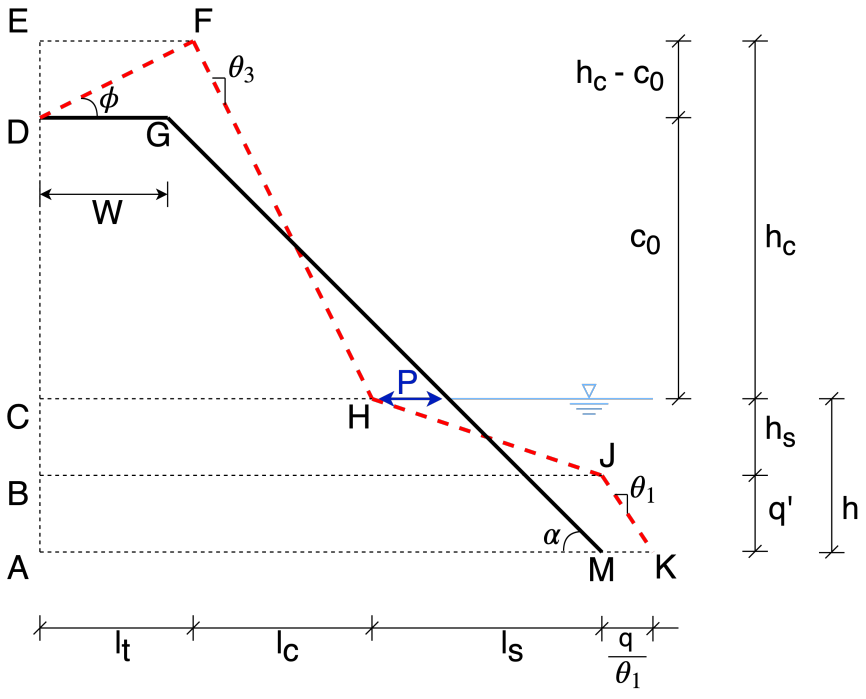

Figure D.1: Schematic overview of the reshaping. The original profile is represented by the thick black line (DGM), the reshaped profile by the dotted red line (DFHJK). The blue arrow shows the horizontal translation of the local origin (H).

High crest levels

For situation the breakwater has a high crest level relative to the water level. Point F, resulting from h_c and l_c can be lower than the top of the crest. To .... the mass-balance the formulas slightly change compared to the one's provided in chapter 5.

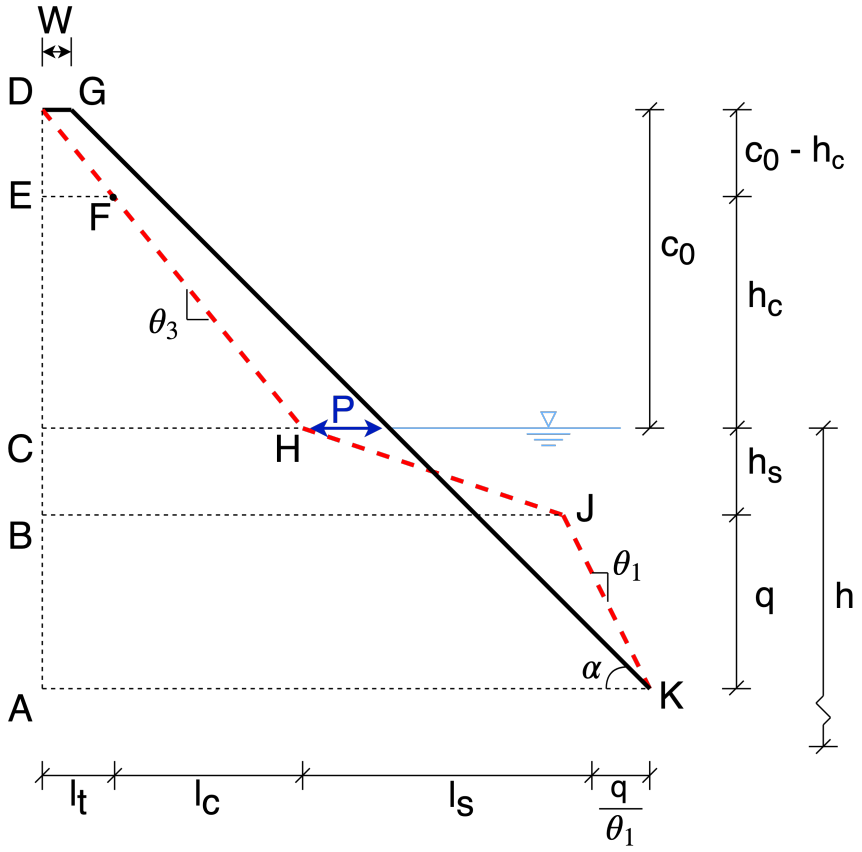

Figure D.2: Schematic overview of the reshaping. The original profile is represented by the thick black line (DGK), the reshaped profile by the dotted red line (DFHJK). The blue arrow shows the horizontal translation of the local origin (H).

D.1.2. Formulas for N

deep water

For plunging waves ($\xi_m < \xi_{cr}$):

$$N_{exposure,pld} = \left[S_d \left(\frac{H_s}{\Delta c_{pl} P^{0.18} D_{n50} \xi_m^{-0.5}} \right)^{-5} \right]^2 \tag{D.1}$$

For surging waves ($\xi_m \geq \xi_{cr}$):

$$N_{exposure,sd} = \left[S_d \left(\frac{H_s}{\Delta c_{s,d} P^{-0.13} D_{n50} \sqrt{\cot \alpha} \xi_m^P} \right)^{-5} \right]^2 \tag{D.2}$$

shallow water

For plunging waves ($\xi_m < \xi_{cr}$):

For surging waves ($\xi_m \geq \xi_{cr}$):

E

Hydraulic boundary conditions

This appendix goes more into depth on the peak selection, to create a new data set with only independent peaks. Furthermore the results from the block maxima method for all the seasons is given.

E.1. Peak selection

To prevent the weekly maximum wave height of two consecutive weeks is induced by the same storm event, it is crucial to separate the data in independent events. The discrete offshore time series is scanned for peaks, and the independent ones are collected in a new dataset, with their corresponding time.

An element of the time series is considered a peak if it is not smaller than its two direct neighbours and larger than at least one of them. Peaks are considered independent if they are at least w locations apart in the time series. In this study w depend on the magnitude of the highest of the neighbouring peaks, such that:

$$w = \begin{cases} w_{min}, & \text{if } y \leq y_{min} \\ w = w_{min} + \dfrac{y - y_{min}}{y_{max} - y_{min}}(w_{max} - w_{min}) & \text{if } y_{min} < y < y_{max} \\ w = w_{max} & \text{if } y \geq y_{max} \end{cases} \tag{E.1}$$

Where the parameters $w_{min}, w_{max}, y_{min}, y_{max}$ are user specified.

E.2. Fitting distribution functions

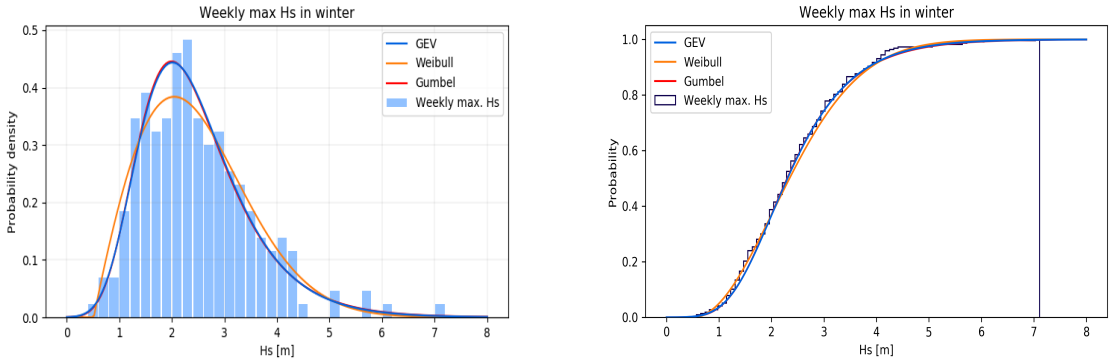

(a) Histogram of the weekly maximum wave heights in winter and the three fitted theoretical probability density functions.

(b) Cumulative distribution of the weekly maximum wave heights in winter and the three fitted theoretical cumulative distribution functions.

Figure E.1: The histogram and cumulative distribution of the weekly maximum wave heights in winter (from time series), compared with the fitted theoretical probability density functions and cumulative distribution functions.

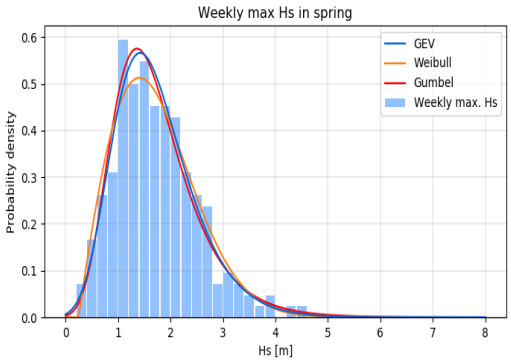

(a) Histogram of the weekly maximum wave heights in spring and the three fitted theoretical probability density functions.

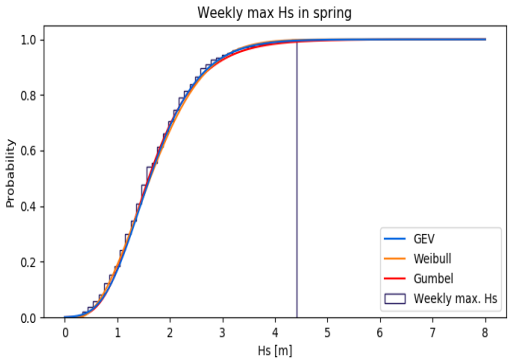

(b) Cumulative distribution of the weekly maximum wave heights in spring and the three fitted theoretical cumulative distribution functions.

Figure E.2: The histogram and cumulative distribution of the weekly maximum wave heights in spring (from time series), compared with the fitted theoretical probability density functions and cumulative distribution functions.

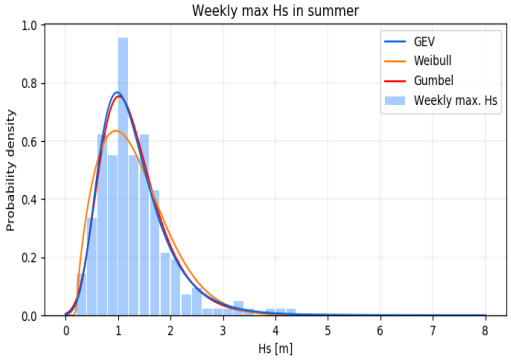

(a) Histogram of the weekly maximum wave heights in summer and the three fitted theoretical probability density functions.

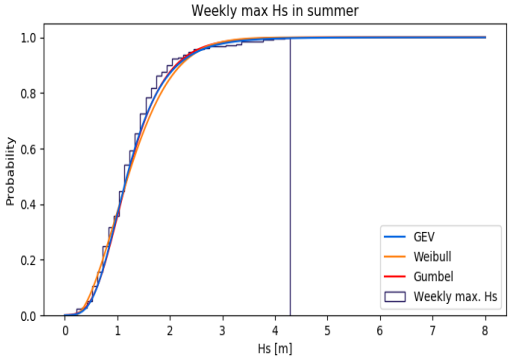

(b) Cumulative distribution of the weekly maximum wave heights in summer and the three fitted theoretical cumulative distribution functions.

Figure E.3: The histogram and cumulative distribution of the weekly maximum wave heights in summer (from time series), compared with the fitted theoretical probability density functions and cumulative distribution functions.

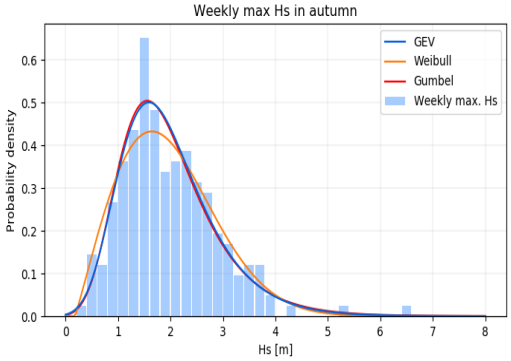

(a) Histogram of the weekly maximum wave heights in autumn and the three fitted theoretical probability density functions.

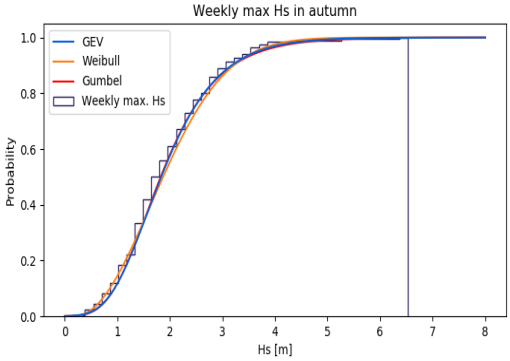

(b) Cumulative distribution of the weekly maximum wave heights in autumn and the three fitted theoretical cumulative distribution functions.

Figure E.4: The histogram and cumulative distribution of the weekly maximum wave heights in autumn (from time series), compared with the fitted theoretical probability density functions and cumulative distribution functions.